POLITECNICO DI TORINO

MASTER'S THESIS

Graphene-based electrodes for neural stimulation and signal recording

Author:
Giorgio AUXILIA

Supervisor:
Dr. Andrea Lamberti

Advisors:
A/Prof. James Fallon
Dr. Joel Villalobos

A thesis submitted in fulfillment of the requirements
for the Master of Science degree in Nanotechnologies for ICTs

at the

Bionics Institute

April 2018

"Allora capii, fui costretto a capire, che fare il dottore è soltanto un mestiere, che la scienza non puoi regalarla alla gente, se non vuoi ammalarti dell'identico male, se non vuoi che il sistema ti pigli per fame"

Fabrizio De André

"Ma s'io avessi capito tutto questo, dati causa e pretesto, forse farei lo stesso"

Francesco Guccini

Abstract

This work is focused on the integration of graphene-based materials with electrodes for neural stimulation and recording of signals. The need for better materials in the field on neuroscience and the growing interest in graphene inspired this study, in which material science and neurotechnology join to develop innovative types of electrodes.
In this thesis the fabrication and characterization of different types of graphene are presented, followed by the results of electrochemical measurements, performed in order to evaluate the properties and performances of graphene-based neuroelectrodes.
We demonstrate that different types of graphene electrodes show different electrochemical properties: in particular single layer graphene and few layer graphene coatings on platinum substrate are not suited for this kind of applications, while porous laser induced graphene networks on polymeric substrate have extremely promising performances for electrical stimulation of neural tissue.

Acknowledgements

I am deeply thankful to James Fallon and to Joel Villalobos for supervising and advising me during these last six months of research at the Bionics Institute. Without their positive attitude when everything seemed hopeless to me and the great guidance in all aspects of the research, I would have not been able to obtain any results and write this thesis.
I also sincerely thank the whole Neurobionics Team for supporting me in this project, in particular Ross, for the help with the design, optimization and realization of the testing chamber, and Mario, for introducing me to the ephemeral world of electrochemistry.

To Andrea Lamberti, which gave me the opportunity of going to Melbourne and joining a vibrant environment such as the Bionics Institute, goes my gratitude: for coordinating the fabrication and characterization of samples performed in Torino and for being the greatest source of ideas and solutions ever imaginable.
A special thank goes to Marco Laurenti, Marco Fontana, Alessio Verna and Stefano Bianco for taking care of the fabrication and characterization of graphene electrode whilst I was abroad.

My whole family, although extremely far in these last months, has always supported me, not only while abroad but always in these past years of university, making the difficult days easier and sharing the bright days.

To Marta, which has been a constant presence in this journey, who shared the burden of hard times and the joy of youth, her bright smile has always encouraged me.

Finally to all my friends that made my university experience unforgettable, from the first day to the thesis.

Contents

Abstract i

Acknowledgements i

1 Introduction 1
- 1.1 Neural Devices . . . 1
- 1.2 Neural electrode technologies . . . 2
- 1.3 Goals and innovative content . . . 2
- 1.4 Thesis content . . . 3

2 Neural electrodes 5
- 2.1 Properties and advantages . . . 6
- 2.2 Disadvantages and Problems . . . 9
- 2.3 Graphene . . . 11
  - 2.3.1 Types of graphene . . . 13
  - 2.3.2 State of Art of Graphene for neural devices . . . 15

3 Methodology 18
- 3.1 Preparation of samples . . . 18
  - 3.1.1 SLG growth and transfer . . . 18
  - 3.1.2 FLG growth . . . 21
  - 3.1.3 LIG . . . 23
- 3.2 Design of testing chamber . . . 26
  - 3.2.1 Testing electrodes: Reference and Counter . . . 27
- 3.3 Electrochemical Measurements . . . 28
  - 3.3.1 Cyclic Voltammetry . . . 28
  - 3.3.2 Electrochemical Impedance Spectroscopy . . . 29
  - 3.3.3 Pulsed Stimulation . . . 31
  - 3.3.4 Accelerated Aging . . . 32

4 Electrochemical characterization 34
- 4.1 Electrochemical measurements . . . 34
  - 4.1.1 Cyclic Voltammetry . . . 34
  - 4.1.2 Electrochemical Impedance Spectroscopy . . . 39
  - 4.1.3 Stimulation pulsing . . . 47

5 Conclusions **51**
5.1 Achievements 51
5.2 Future outlook 52

Bibliography **54**

List of Figures

2.1 Examples and evolution of neural electrodes: a glass micropipette [17]; a planar array coated and uncoated platinum disk electrodes; a 22 electrodes cochlear array; a penetrating silicon multi-electrode array (Blackrock Microsystems). 6
2.2 Examples of neurostimulation devices: a) cardiac pacemaker [57]; b) bionic eye; c) cochlear implant; d) deep-brain-stimulation apparatus. 7
2.3 a) Utah probe with sputtered Iridium Oxide exposed on the tip, [44]; b) platinum electrodes from a cochlear array c) coated with a conductive hydrogel [27]; d) schematics of coatings with CNT, conductive polymers and hydrogels and bioactive molecules [2]. 9
2.4 Graphene and its derivatives: a fullerene, a single-wall nanotube and graphite, [31] 12
2.5 Graphene barrier used in water desalination [13]. 13
2.6 Applications of graphene in neuroscience: I) comparison of neuronal growth on graphene and on control substrate [8]; II) fabrication process of SLG on gold substrate [32]; III) fabrication steps and images of LIG electrodes and gold tracks for cortical microstimulation [37]; IV) Development of neural activity with time on graphene substrate [54]. 16

3.1 Transfer process of single layer graphene on platinum electrodes. 19
3.2 Transfer process of single layer graphene on platinum electrodes. 19
3.3 Comparison between typical spectrum of SLG and that measured on copper film before the transfer process. 20
3.4 Comparison of Raman spectra of two different regions on a platinum disk. 21
3.5 FESEM images of platinum foils at different growth times: [0, 60, 120, 300] s. (SE2 detector) 22
3.6 Raman spectra at different deposition times of graphene grown on platinum. 22
3.7 Fesem images of graphene on platinum at different growing times with observable graphene features. 23
3.8 Comparison of cyclic voltammetries results for different LIG morphologies [34]. 24
3.9 Low and high magnification FESEM images of LIG samples, [34]. 24
3.10 Raman spectrum of LIG samples with different morphology, [34]. 25

3.11 Process sequence of LIG electrodes: writing, doping, PDMS coating and peeling, transferred LIG electrodes [49]. 26
3.12 CAD images and real picture of the testing chamber. 26
3.13 Generic cyclic voltammogram with the current response to the driving applied voltage [41]. 28
3.14 Small AC voltage perturbation and the consequent current response. . . . 30
3.15 Time-dependent representation of excitation AC voltage and recorded AC current with focus on the frequency-shift. 30
3.16 Current and voltage pulses with pulse width of 500 µs 32
3.17 Simulation of accelerated aging at 90 °C with aging coefficients of 1,8 and 2,0. 33

4.1 Comparison of CVs of platinum electrodes with different exposed area . . 35
4.2 Comparison of single layer graphene, few layers graphene and platinum electrodes' voltammograms. 36
4.3 Picture of LIG electrode with inset on the exposure hole and platinum collector. 37
4.4 Comparison of CV curves for LIG and platinum electrodes. 37
4.5 Comparison between CVs of LIG before and after activation. 38
4.6 Comparison of CSC values for platinum, LIG and activated-LIG. 39
4.7 Comparison of CV curves of a LIG electrode at day 0, day 6 and day 13 of accelerated aging protocol. 40
4.8 Comparison of aged LIG samples with platinum and unactivated LIG. . . 40
4.9 Comparison of EIS modulus for different sizes of platinum electrodes. . . 41
4.10 Comparison of EIS modulus between platinum and graphene-coated electrodes. 42
4.11 Comparison of EIS measurements for all four types of electrodes at 1 kHz. 43
4.12 Comparison of EIS modulus for the same LIG electrode before and after activation and during accelerated aging. 43
4.13 Comparison of EIS modulus between platinum, unactivated LIG and activated LIG at day 0, 6 and 13 of the aging protocol. 44
4.14 Placement of platinum collector with respect to LIG exposed electrode. . . 45
4.15 Vertical shift of the modulus of the EIS due to the increased resistivity given by the LIG tracks. 45
4.16 Comparison of EIS values for samples 46
4.17 Comparison of CSC values. 47
4.18 LIG response to stimulation pulse with E_{mc} equal to -1.2V and 0.6 V. . . . 49
4.19 50

List of Abbreviations

CIC	**C**harge **I**injection **C**apacity
CSC	**C**harge **S**torage **C**apacity
CVD	**C**hemical **V**apor **D**eposition
CV	**C**yclic **V**oltammetry
EIS	**E**lectrochemical **I**mpedance **S**pectroscopy
FLG	**F**ew **L**ayers **G**raphene
LIG	**L**aser **I**nduced **G**raphene
PBS	**P**hosphate-**B**uffered **S**aline
PDMS	**P**oly**di****m**ethyl**s**iloxane
PEDOT	**p**oly(3,4-**e**thylene**dio**xy**t**hiophene)
PMMA	**P**oly(**m**ethyl **m**eth**a**crylate)
SLG	**S**ingle **L**ayer **G**raphene

Chapter 1

Introduction

Neurotechnology is the science related to the study and understanding of the intimate relation between an electrically active cell, the neuron, and an external microelectronic system. Neurotechnology has three major areas of application: neuroscience, which aim is to investigate the basic principles behind the neuronal interactions and reactions to stimuli; neuroprosthetics, which deals with the artificial restoration or replacement of damaged parts or functions of the nervous system [3]; and neuromodulation, in which the behavior and functions of the nervous system are modified.

1.1 Neural Devices

Medical bionics and neural prosthetics have been used for many years to improve quality of life of millions of people with neurological deficiencies. Neural electrodes are currently used to artificially stimulate neural tissue and record activity in many different fields of application. Electrical stimulation is used to activate or modulate the neurons, with the aim of driving the defective pathway in a useful manner and restore the neural function and activity, both for sensory deficits or motor inefficiency.

Any implant contains many different components, besides the electrodes, which are the actual part that interfaces with the neural tissue: a whole set of other components are required to create a fully working implantable device. The electrodes must be connected to the external world through cables, which must have low resistivity, in order to dissipate the least amount of power. Flexibility also plays a fundamental role in implantable devices, which leads to the choice of materials able to guarantee a good electrical connection while keeping good mechanical properties. This property will be further discussed in the following chapters. Other key elements to the performance of the device are the implantable electronics that are needed to perform the actual stimulation or recording of signals, such as amplifiers and filters for the recorded signal, and an external processing unit that drives the functioning of the whole implant. Ultimately, a power supply source is needed to provide the energy required to perform all activities within the implant: in portable devices the capability of the battery must be tailored to the needs and ensure the necessary lifetime.

1.2 Neural electrode technologies

Electrodes used for neural applications must meet many different requirements in order to effectively stimulate and activate the neural response or to record a signal, but at the same time they must be safe for the biological environment in which they are inserted. In each stimulation cycle, charge is exchanged between the electrode and the neural tissue, causing a functional response through the depolarization of the cell membrane [12].

The requirements for implantable electrodes are not limited only to electrochemical properties, but most importantly they must be safe for the patient and not harmful for the physiological environment. All materials have to be biocompatible and biostable and non toxic to biological environments; for any in vivo application, the electrode will be exposed to higher temperature than normal ambient temperature, to organic species that may attach to its surface and to the physiological response toward the foreign body that will lead to scarring tissue formation and encapsulation.

All these factors have to be taken into account and possibly avoided and the choice of the material plays a fundamental role. Most implants at present use electrodes made of noble metals such as platinum or iridium for these reasons: they are highly conductive but at the same time chemically inert and do not degrade easily in biological environments. Other materials frequently employed are iridium oxide, mainly for recording, and titanium nitride or tantalum oxide, which are used in stimulation applications.

One key requirement for electrodes implanted in the body is long term stability: when subjected to continuous pulsed stimulation, the material undergoes chemical reactions of oxidation and reduction, that may produce unwanted species that might be harmful when released in the environment. Moreover the electrode should not degrade over time, releasing micro or nanoparticles that are not biodegradable and can accumulate in the tissues or organs.

1.3 Goals and innovative content

This work describes the studies made to evaluate the improvements that the integration of graphene, a single atom thick two-dimensional material with atoms arranged in a honeycomb pattern, and its structures could provide in implantable electrodes. The standard material for implantable electrodes and devices is, at present and in the last decades, platinum due to its good electrical conductivity, its high inertness and biocompatibility being a noble metal. However, metallic electrodes, even if biocompatible and non toxic such as platinum, exhibit many limitations for neurotechnology implants, mainly for what concerns the mechanical mismatch between the rigid electrode and the soft neural tissue, which causes scarring and encapsulation of the device, strongly reducing the effective

properties of the implant.

Graphene has been studied thoroughly in the last decade since its discovery in most fields of applied physics and material science, in order to try to apply its outstanding properties in different types of applications. The innovation studies in neuroscience have always been focused on the research of innovative materials that could solve some of the problems that the use of platinum electrodes presents. Due to its properties, graphene is thought to be a valuable candidate to improve the properties of neural electrodes, both in terms of electrical and electrochemical properties, for what concerns biocompatibility and biostability and for its mechanical features of flexibility, elasticity and strength.

In the present study three different types of graphene structures have been fabricated, characterized and studied in order to evaluate the electrochemical properties and the feasibility of integration into neural devices.
The first two types of graphene-based electrodes employed a platinum substrate which guaranteed mechanical support and electrical connection: the differences between a bare platinum electrode and the same material coated with a carbon-based bidimensional film have been evaluated.
The third material did not employ any metallic substrate, creating graphene-only electrodes on a polymeric foil as support, allowing for a greater versatility in term of customization, fabrication and flexibility with respect to standard platinum electrodes. It consists on a directly-written porous network of graphene flakes on a polyimide substrate.

1.4 Thesis content

This thesis will present the work performed in collaboration between the Politecnico di Torino and the Bionics Institute of Melbourne, to evaluate the possibilities of integrating graphene onto implantable devices for neural stimulation and recording of signals. In the next chapter the case study will be presented, briefly showing the history of stimulation and recording implantable devices, their evolution in relation to the required properties and the current state of the art. Moreover a brief introduction of graphene, its properties, the fabrication and characterization techniques will be presented, followed by the few applications of graphene in the field of neuroscience and technology.

In chapter 3, the techniques employed to fabricate and characterize the materials for all types of graphene will be presented and explained, focusing on the differences between the techniques and properties of the various graphene-based materials. The design and realization of the measurement apparatus and the theoretical background on electrochemical measurements is also described in the following chapter.

In chapter 4 the results of the measurements will be presented, focusing on the most relevant parameters that can be extracted from each experiment. The data of cyclic voltammetry, electrochemical impedance spectroscopy and stimulation pulsing will be presented for each type of electrode and compared to platinum samples tested in the same conditions, allowing for a reliable internal control.
Finally, the conclusions about the achievements and a synthesis of the relevant results are presented along with the future outlook that arises from the present work.

Chapter 2

Neural electrodes

Since long times the scientific community has tried to develop implantable devices capable of interacting with the tissues and cells of the nervous system.

The first types of microelectrodes for neurophysiological applications were glass micropipettes, figure 2.1a, filled with an electrolyte, with a very small diameter, in the order of few micrometers, that were used in intracellular applications. Later metallic microelectrodes appeared, which had lower impedance and higher polarization potential, figure 2.1b, and were mostly employed to record extracellular signals [3].

Prosthetic implants were developed later and the first implantable stimulation device was the internal pacemaker in 1958, although not properly a neuro-device, it is still the most successful implantable device figure 2.2a. The first motor prosthesis for foot drop in hemiplegics appeared in 1962 [26] and since then the neurotechnology industry grew exponentially and reached more than 8 billions dollars in 2012 [7].

Implantable electrodes have been used for many years for patients affected by deafness by implanting an array of electrodes in the cochlea (inner ear) figure 2.2c: from the first cochlear implant, developed in 1957, the diffusion of this kind of device has grown vastly and as of 2012, there were over 300,000 patients with a cochlear implant [28]. Another successful implantable device, the bionic eye, consists in an implantable array of electrodes placed behind the retina, figure 2.2b, to stimulate the optic nerve and to restore the vision in blind patients affected by retinis pigmentosa [39]. Stimulation of neural tissue is also used to restore or improve communication between the brain and the gut through the stimulation of the vagus nerve to increase the anti-inflammatory response of the vagus nerve and to treat patients with epilepsy or Crohn's Disease [5]. Other types of neurostimulation devices include Deep-brain-stimulators (DBS) figure 2.2d which are effectively used to improve the quality of life of people affected by essential tremors, Parkinson's disease or dystonia.

Electrodes arrays are used both to detect and to evoke electrical neural signals. Recording arrays are interfaced with an external system that records and analyzes the acquired

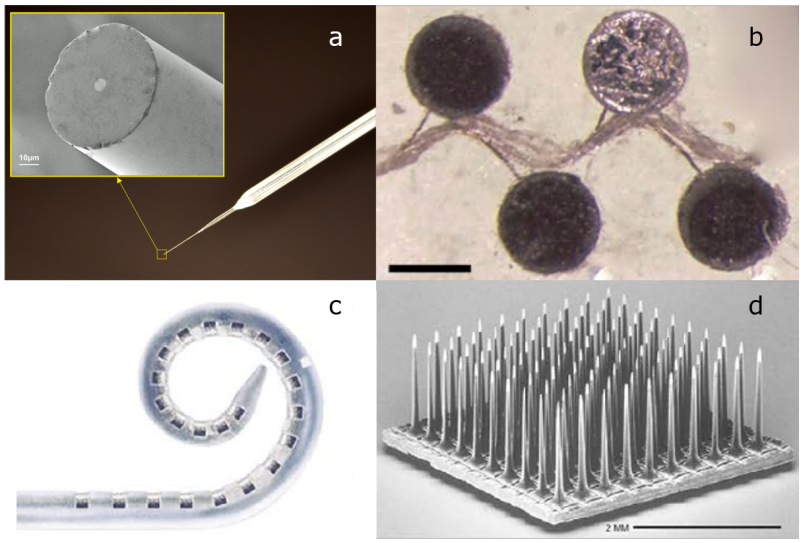

FIGURE 2.1: Examples and evolution of neural electrodes: a glass micropipette [17]; a planar array coated and uncoated platinum disk electrodes; a 22 electrodes cochlear array; a penetrating silicon multi-electrode array (Blackrock Microsystems).

signal and they are used to understand the behavior of the nervous system. Brain Machine Interface, also known as brain computer interface, is a growing and promising field of research that aims at the understanding of neural signals to control robotic prosthetic limbs through conscious activity of the central nervous system [48] [35].

2.1 Properties and advantages

Recording and stimulating electrode arrays have many similar requirements from the safety and stability point of view, but differ for what concerns the electrochemical required properties. From the electrical point of view, the most important parameter is the electrochemical impedance, which is usually measured in the 1 Hz-100 kHz range, and the most important figure of merit is the impedance around the 1 kHz frequency. Recording neural implants usually have low electrochemical impedance in the range of frequency used for biological and medical applications to be able to detect small variations of potential in the neural tissue, of the order of few hundreds of millivolts. However the impedance can also be purposely increased to enhance the spatial resolution and record signals from a very limited number of cells.

Concerning stimulating electrodes, they are usually described by the charge storage capacity (CSC) being a measure of the amount of charge that can be stored and it represents an upper limit for the charge that can be delivered during a stimulation pulse. It is calculated integrating the cathodal current with respect to the voltage sweep rate of a cyclic voltammogram[1]. Charge injection capacity is a measure of how much charge can

[1]More details on cyclic voltammetry and charge storage capacity will be given in chapter 3.

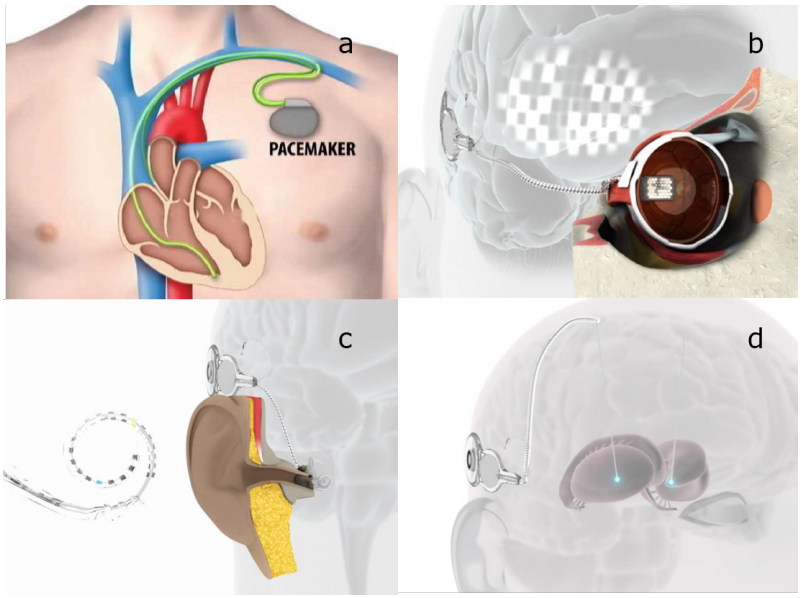

FIGURE 2.2: Examples of neurostimulation devices: a) cardiac pacemaker [57]; b) bionic eye; c) cochlear implant; d) deep-brain-stimulation apparatus.

be injected during a single stimulation pulse to the neural tissue. The most important requirement for stimulating electrodes is the safety of the charge injection process. For each material, the electrode potential excursion must be evaluated in order to determine the water window. Polarization of electrodes at higher potential values would induce electrolysis of water, generating H^+ ions which can cause a shift in pH that can be extremely dangerous for tissues [30].

Many attempts and studies have been made in order to improve the properties of neural electrodes and implants or to solve problems and defects. Among the most common drawbacks are the limited amount of safely injectable charge that limits the range of non-damaging stimulation and the inflammatory response toward the implant that limits its efficacy. Most of the attempted strategies to increase the performances of electrodes are based on the employment of different materials that modify the surface properties of the electrode, the only part being in direct contact with the biological environment.

Most implants today use electrodes made of noble metals such as platinum or iridium because they are highly conductive but at the same time chemically inert and do not degrade easily in biological environments.

New materials have been employed as coatings to metallic electrodes in order to increase the electrochemical properties of the implants and to expand the safe charge-injection limits. Iridium oxide has been proven to be a very promising material for intracortical applications with charge injection capacity larger than noble metals [11], that is grown on an iridium electrode through successive oxidation and reduction cycles, forming a hydrated oxide film on the surface.

Alternatively, Negi et al. demonstrated that iridium oxide could be sputtered on the tips of microelectrodes of the Utah probe figure 2.3a and that it could be successively activated to form through pulsing in phosphate buffered saline (PBS) [44]; he tested the stability of both coatings during prolonged stimulation, showing that sputtered iridium oxide films have a higher damage threshold and are a better candidate for chronic applications.
Other materials frequently employed are titanium nitride or tantalum oxide, which are used in stimulation applications.

Many studies on coatings for neural electrodes focused on organic molecules to try to reduce the mechanical mismatch between the metallic electrode and the neural tissue, while maintaining good electrical properties. Conducting polymers (CPs) have been studied for decades due to their low Young's modulus, their swelling nature in aqueous environments and the ease of functionalization, making them very suitable for neural interfaced devices [9]. Green et al. performed numerous studies on conductive polymers, in particular poly-ethylene dioxythiophene (PEDOT), polypyrrole (PPy) and polythiophene (PTy) [24], characterizing the electrical properties [22] and the mechanical behavior. They later focused on the stability of the CP in dependence from the underlying metallic substrate, showing that a roughened surface did not compromise the electrochemical properties while greatly increasing the stability and lifetime of the conducting polymer in chronic stimulation conditions [25].

Studies by Hassarati et al. used conductive hydrogels in cochlear implants to improve the interfacial properties and reducing the scarring caused by the dissimilarity in mechanical properties figure 2.3c, while increasing the charge storage capacity of 37% with respect to bare platinum [27]. The same study showed that conductive hydrogels coating could increase the charge injection limits of roughly one order of magnitude with respect to platinum for a 200 µs phase width pulse. Green et al. combined the two technologies proposing polymer-hydrogel hybrids with conductive capability, with the aim of improving the relatively poor mechanical properties of polymers through the use of hydrogels, intercalated with highly conductive polymers such as PEDOT [23].

Others worked on the miniaturization and on the surface modification of electrodes, mainly to increase the effective surface area without changing the geometrical surface area [43], being able to increase the charge injection capacity up to 80 times with respect to unmodified samples.

Nanostructures have been studied as possible solutions to reduce the size of the electrodes to minimize the impact of invasive implants, while guaranteeing sufficient electrochemical properties for stimulation or recording. Ryu et al. used ZnO nanowires

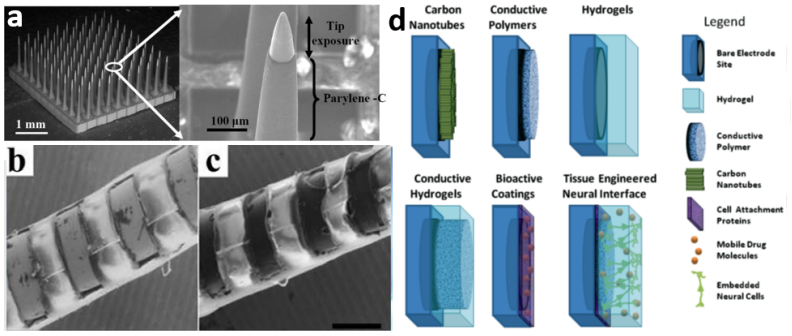

FIGURE 2.3: a) Utah probe with sputtered Iridium Oxide exposed on the tip, [44]; b) platinum electrodes from a cochlear array c) coated with a conductive hydrogel [27]; d) schematics of coatings with CNT, conductive polymers and hydrogels and bioactive molecules [2].

coated with PEDOT on a flexible substrate, with graphene-based interconnections to realize low impedance recording probes [48]. Carbon-based electrodes and coatings have been widely studied due to the properties of carbon allotropes, the great biocompatibility and non-toxicity, the conductivity and stability.
Besides the conducting polymers of above, also diamond has been studied as a stimulating electrode material. Garrett et al. studied the properties of nitrogen-doped ultrananocrystalline diamond, showing good charge injection capacity [21]. Carbon nanotubes, figure 2.3d, have been studied as a possible solution to improve the electrochemical properties of electrodes by increasing the effective surface area, or to provide better mechanical stability to conductive polymers or hydrogels [2]. Lastly, also graphene, being closely linked to single-wall carbon nanotubes, has been studied for neural applications as will be shown in the next section.

2.2 Disadvantages and Problems

Besides the electrochemical properties, implantable devices must satisfy stringent safety requirements, in order not to bring harm to the patient and to the biological environment. The biocompatibility and biostability of implants play a major role in the functioning of the device, avoiding any damage to the physiological system and ensuring the minimal response from the body that would lead to formation of unwanted tissue, decreasing the device's performances.

One key requirement for electrodes implanted in the body is long term stability: when subjected to continuous pulsed stimulation, the material undergoes chemical reactions of oxidation and reduction, that may produce unwanted species that, released in the environment, might be harmful. Moreover the electrode should not degrade over time, releasing micro or nanoparticles that are not biodegradable and can accumulate in the tissues or organs.

It has been shown how the scientific community have been studying different solutions and options to obtain efficient and safe devices for neural stimulation and recording for decades. However the optimal solution is yet to be found under many different aspects, from the ability to inject charge or record signals from the biological tissue, to the safety and stability of the implants. Coating of metallic electrodes with different materials to change the superficial properties of the electrode has proven to be an effective solution, but the optimal material has not been found yet. Therefore new innovative materials such as graphene and graphene-related materials could provide a viable solution to increase the performances of neural implantable devices.

2.3 Graphene

Graphene is an allotropic form of carbon consisting of sheets that extend in 2 dimensions and have the thickness of one atom. It is one of the most innovative and disruptive material recently appeared on the theoretical and applied physics and engineering scene. It has been studied for many years, but in the 1930s, Landau and Peierls predicted that a fully 2-D material could not exist according to the idea that thermal fluctuations in low-dimensionality structures would be comparable to the interatomic distance and make the crystal lattice unstable. Therefore graphene, and in general 2D crystals, has been considered for many decades only as academic material, that could not exist in free state. In 2004 graphene was discovered by Novoselov et al. and ever since it has been studied thoroughly in order to empirically demonstrate its theoretically predicted properties [45]. It is the first material to be artificially synthesized that is fully two-dimensional and it can be considered as the source of other carbon allotropes: fullerenes, single-walled carbon nanotubes and graphite, figure 2.4. Due to its outstanding properties, it has been employed in a plethora of application fields in material sciences.

Graphene has brought a revolution in the research of fundamental properties of condensed matter; due to its lattice configuration and electronic structure graphene exhibits quantum Hall effect also at room temperature and the nature of its carriers is unique. The dispersion relation close to the Fermi level is linear, therefore electrons and holes are moving with zero effective mass. They are better described by the Dirac equation than the Schrödinger, being massless relativistic quasi-particles, called Dirac fermions. This relativistic description of electron waves has been theoretically studied for many years, and since the discovery of graphene many efforts have been made to measure these quantum electrodynamic phenomena, [31].

Due to the revolutionary characteristics of graphene, it is employed in many different fields. First of all in electronics and electronic devices, also because of the large investments of electronic corporations such as Intel or IBM. Graphene is thought to be as one of the most promising material to substitute silicon-based technology, being CMOS electronics almost at its fundamental limits. It has been used because of its electron mobility, higher than metals, up to $10^5\,cm^2/Vs$ at room temperature. Moreover mobility does not degrade even at high electrical-doping levels and it is almost not affected by chemical doping. These properties ensure ballistic transport at room temperature on a submicrometric scale. Graphene is a zero energy-gap semiconductor which could be used, not only as a FET channel material, but also as a conductive sheet in single-electron-transistors.

The most interesting features of graphene, though, go beyond the simple electrical properties. It combines transparency, good heat conduction and great mechanical properties, such as elasticity and flexibility. It is chemically inert and highly stable, making it a suitable candidate to substitute current transparent conductors, such as ITO (indium tin oxide), in the next generation of transparent devices.

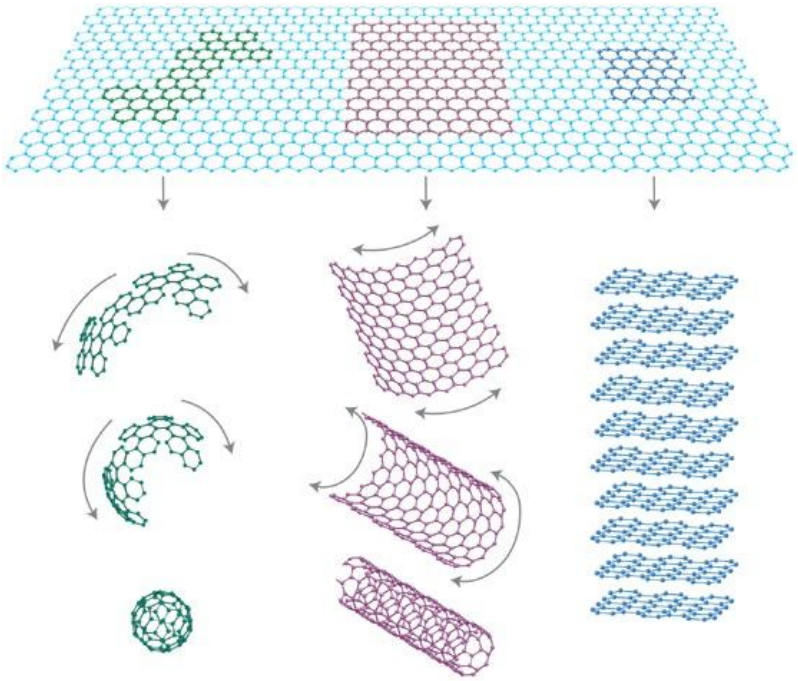

FIGURE 2.4: Graphene and its derivatives: a fullerene, a single-wall nanotube and graphite, [31]

Due to the many different properties that graphene and graphene-related-materials have, they can be applied in a broad spectrum of areas: innovative energy solutions, both for energy storage and generation. The unique optical properties, the great carrier mobility, the thickness and mechanical robustness and elasticity make them suitable both for innovative photovoltaic and fuel cells and for supercapacitors, batteries and hydrogen storage [10] [1].

Its applications go beyond simple electronics and energy storage and generation, it can combine them to create optoelectronic or spintronic devices, or to realize sensors for health and environment. Graphene and graphene-oxide membranes have employed in liquid separation applications, such as desalination [13], water filtration and lab-on-chip microfluidic systems, since the graphene layer, when opportunely patterned with nanopores , allows the flow of water molecules while stopping larger ions and molecules as in figure 2.5.

The broadness of possible usages of graphene is reflected in the multiple fields and sectors of patents [20]. As of 2014, more than a quarter of patents were related to the synthesis and production of graphene itself, being a relatively new technology that needed to develop reliable and commercially available techniques for mass production. As previously stated, large part of the market is occupied by electronics, but almost 50% of patents until 2014 were filed for other applications, such as composite materials, energy and health.

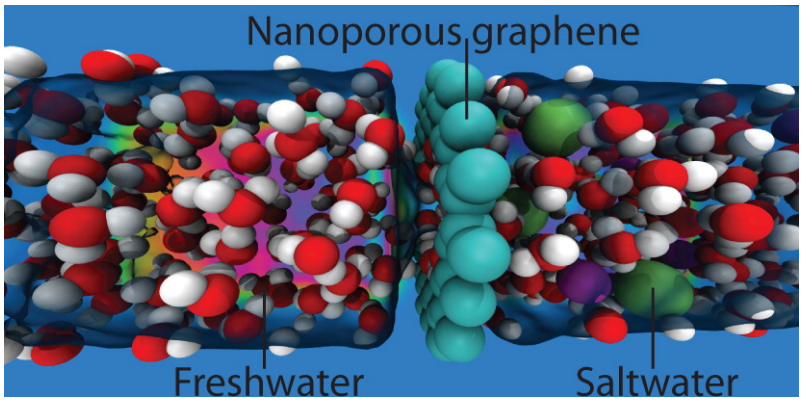

FIGURE 2.5: Graphene barrier used in water desalination [13].

2.3.1 Types of graphene

SLG/FLG Among all graphene related materials, the proper form is the single layer graphene (SLG), which is the only fully two-dimensional material among the GRMs. It has been discovered and isolated for the first time by Novoselov and Geim, through a micromechanical cleavage process of bulk graphite [45]. By repeated peeling of small masses of highly-oriented pyrolytic graphite, they were able to prepare single-layer graphene and few-layers graphene (FLG) samples with high reliability and large areas, up to 10 µm. This mechanical exfoliation process presented the first reproducible and simple technique to prepare two-dimensional crystals of graphene.

One of the advantages of graphene is that it can be produced in many different ways, in a large scale and with limited costs, both with bottom-up and a top-down approaches. Among the top-down techniques, in which material is removed starting from bulk to obtain the final product, besides the micromechanical cleavage used by Novoselov and Geim, are the liquid-phase exfoliation of graphite or graphene-oxide, in which an ultrasound source is used to disperse in liquid individual layers of graphene, and anodic bonding, in which a graphite layer is pressed onto a glass substrate and, through the application of a large voltage and high temperature, SLG flakes bound to the glass by electrostatic interaction and can be subsequently isolated [20].

The most common techniques for the growth of graphene films onto a planar substrate, with a bottom-up approach, are the epitaxial growth on SiC wafers and the chemical vapor deposition (CVD). Graphene growth on silicon carbide wafers is given by the rearrangement of carbon atoms on the surface as the silicon evaporates from the substrate. The most common technique, although, is the CVD, which allows to grow high quality and large area samples for all applications that need a continuous film with large area and high crystallinity. In chemical vapor deposition a gaseous precursor containing the material to be deposited, in this case carbon, is flown into the reaction chamber. It is then decomposed by heat, or other energy sources, and the carbon atoms nucleate on the surface of the substrate, forming the monolayer. The substrate is usually a metal that acts as a catalyst for the nucleation reaction, mostly copper, since it is relatively cheap and the grown domains are large if compared to other substrates.

The graphene layer is then transferred to the the final support through the etch of the copper film and the ease of the copper etching process makes it even a better candidate as graphene growth substrate.

Also platinum can be used as a metallic substrate for the growth of graphene by carbon segregation on the surface. The result is a continuous single layer with some wrinkles in the graphene sheet given by the thermal stress and the lattice mismatch between crystalline platinum and graphene. At the edges of the SLG domains, few-layers graphene regions are often found, [53]. The definition of few layers is based on the properties of the material. Obviously a single layer is a two-dimensional structure, but how many layers are needed to create a 3D material? For the case of graphene, the limit is based on the properties of the electronic structures, which evolves from a zero band-gap semiconductor, in case of a single layer, to the electronic structure of graphite when there are more than ten layers, [46].
Often, as analyzed by Winnterlin and Bocquet, the multilayer regions are due to carbon atoms underneath the graphene layer, locally bound to the underlying metal, covered and trapped by the graphene sheet, [56]. This problem can be avoided by using highly oriented crystalline platinum thin films as a substrate, as done by Nam et al. with LP-CVD process, [42].

LIG Laser Induced Graphene is a material derived from the graphitization of a polymer through a laser source. The first studies on the laser writing of polyimide (PI) were conducted in the late eighties by [50], who focused on the properties of the obtained material and of the process parameters to obtain an effective etch of the Kapton film.

Later works, conducted by Brannon and Srinivasan, studied the laser sources, CO_2 [6] and UV [51], and the absorption of the radiation in the material, the energy involved in the etching process and the gaseous byproducts of the process.

Davenas optimized the laser parameters, power and scan speed necessary to obtain a highly conductive nanostructure based on carbon atoms [15]. These preliminary works, although quite promising in terms of realization of microelectronic devices , were almost forgotten until 2012 when the properties of laser induced graphene seemed extremely suitable in the field of wearable and flexible electronics. Strong et al. proposed an innovative way to produce a carbon based material in a single step through the reduction of graphene oxide. GO is an ideal starting material for the production of large scale graphene-based material, but the oxygen species make it non conductive, therefore multiple techniques were proposed to reduce GO and re-establish the conjugated carbon-carbon bonds. The process proposed did not require expensive equipments or high temperatures, instead it was based on the use of a standard DVD optical drive controlled by a LightScribe software. Using a 788 nm infrared laser source, they were able to directly pattern the conductive structure, controlling the sheet resistance and the conductivity simply by tuning the laser power, [52].

The first definition of Laser-Induced-Graphene was made by Lin, that, using the studies by Brannon et al. on CO_2 laser ablation of polyimide, fully and thoroughly characterized the obtained material, showing that it was a porous structure of graphene flakes, [36]. The production process involves the local heating of the PI film through laser irradiation to elevated temperatures, up to 2500 °C . This causes the bonds in the polymeric chain to break and the release of oxygen and nitrogen gaseous species, while the carbon atoms rearrange to form sp^2-hybridized planar structures typical of graphene. Tuning the radiation power, the frequency of the pulsed laser and the scan rate, it is possible to optimize the graphenization process and change the properties of the LIG. A minimum amount of power is required to start the carbonization of the polymer via photothermal effect, while the upper limit is given by the oxidation of carbon that can degrade the LIG quality.

The characterization of the material showed that the underlying PI film was not damaged and offered structural support to the foamy-like porous material. [34] characterization is performed through electron microscopy (FESEM) to determine the morphology of the LIG structure in dependence on the writing parameters (frequency and scan-rate). To determine the composition of the carbonized structure, x-ray photoelectron spectroscopy (XPS) and Raman spectroscopy can be employed, while x-ray diffraction (XRD) spectra are used to determine the crystalline structure and the dimensions of the flakes of graphene [2].

Given the particular properties of the LIG, it has been used in a broad range of different applications that exploited its relatively large conductivity associated to the large surface area, the flexibility and the ease of production in single-step processes. For example it has been widely used in the field of energy storage to realize micro supercapacitors [33] and [49], reaching values of specific capacitance above 750 µF cm^{-2}, to produce strain sensors [38] or create health diagnostic systems, such as blood analysis tests [18], or water splitting electrodes [58].

2.3.2 State of Art of Graphene for neural devices

Graphene and related materials have been employed in many studies in the field of neuroscience and neuroprosthetics, not only because of their excellent properties, but also since it has been proven to have a good biocompatibility and low toxicity toward biological environments.

The promising properties of graphene, in terms of biocompatibility, electrical conductivity and mechanical strength are suitable both for stimulation and recording of neuronal cells. In their study, Koerbitzer et al. show that coating gold and silicon dioxide with single layer graphene, figure 2.6II, improved the stimulation capability of the electrode, reducing the electrochemical impedance and ensuring a large charge injection and charge storage capacity [32]. Electrical stimulation can be used not only to directly evoke an action potential and firing of the neuron, but also increase the cell-to-cell interaction

[2] More on electron microscopy and Raman spectroscopy will be explained in the methods chapter of this thesis.

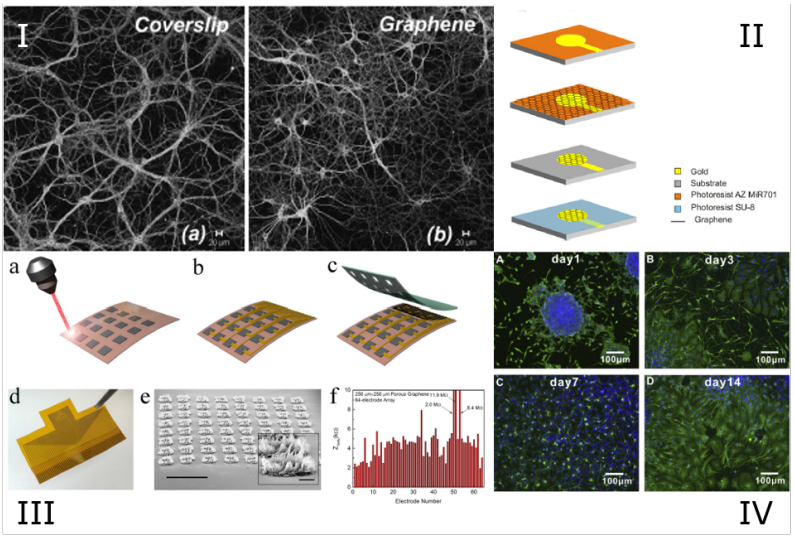

FIGURE 2.6: Applications of graphene in neuroscience: I) comparison of neuronal growth on graphene and on control substrate [8]; II) fabrication process of SLG on gold substrate [32]; III) fabrication steps and images of LIG electrodes and gold tracks for cortical microstimulation [37]; IV) Development of neural activity with time on graphene substrate [54].

in neural system. A non-contact weak electric field stimulation of neuron networks on graphene layers induced an increase in the number of neurons' pairings and strengthening of preexisting coupling, [29].

Graphene electrodes can also be used to record the spontaneous electrical activity of neural cells. Du et al. demonstrated a reliable way to fabricate graphene micro-electrode arrays (MEAs) and tested their long term stability. Cortical cells were cultured for 40 days and a comparison in electrochemical impedance before and after was made. They showed that graphene microelectrodes do not suffer from long exposure times in neurological environments and the good biocompatibility of graphene [16]. Not only graphene is demonstrated to be able to withstand long term exposures to neural tissue cultures, but it also improves the formation of neural networks, figure 2.6IV. Tang et al. showed that graphene films could be used as scaffold to favor the growth of networks in neural stem cell culture, which represents a very promising technique to reconstruct damaged neural circuits and tracts [54]. Ultimately, graphene membranes have also been used to record the action potential of nerve fibers, which has potential direct applications in neuroprosthetics. Chen used a graphene-on-silicon dioxide electrode to record the activity of a lateral giant nerve fiber, figure 2.6I. The same electrode has been tested in vitro to evaluate its properties, with electrochemical impedance modulus as low as 117 kΩ at 1 kilohertz and charge storage capacity of 0.65 µF cm^{-2} , and in vivo on a crayfish, with action potentials of amplitude V_{pp}=162 µV and SNR above 30 dB [8].

Lu et al. demonstrated that an array of porous graphene could be used for neural stimulation applications [37]. They realized a 64-electrodes array of LIG on polyimide

through laser irradiation, connected with sputtered gold lines, insulated with a SU-8 encapsulation layer, figure 2.6III. They showed that LIG electrodes during in-vitro measurements performed better than gold electrodes, decreasing impedance and increasing the charge storage and injection capacity. The measurements performed in-vivo showed good recording and stimulation properties, even though no chronic implantation was performed, in which the stability of performances and durability of the implant would have been evaluated.

Chapter 3

Methodology

The procedures and methods used to carry out the experiments will be presented in this chapter. First it will be explained how the tested samples have been prepared, followed by design of the experimental apparatus and the theory of the proposed experiments.

3.1 Preparation of samples

The electrodes that will be analyzed can be divided in those based on a platinum substrate, such as the single layer graphene and few layers graphene on platinum, and those that do not contain any metallic substrate, which is laser induced graphene on a polyimide film.

3.1.1 SLG growth and transfer

The first kind of samples is based on platinum electrodes, shaped as thin disks, that have been covered by single-layer-graphene.

Starting from commercially available platinum foil[1] of 50 µm in thickness, disk-shaped electrodes were obtained punching the foil and obtaining an electrode with a diameter of 600 µm.
The single layer graphene was previously grown on a copper foil through a chemical vapor deposition (CVD) process. The substrate is a commercial Cu foil[2] which is first cleaned in 10 % HCl aqueous solution to remove impurities and native copper oxide and then dried in nitrogen flow. The freshly cleaned copper foil was loaded in the cold-wall CVD reactor (NANOCVD 8-G system from Moorfield) and placed directly over the substrate heater. The first step of the growth is an annealing step of the sample for 10 minutes at 1000 °C in pure argon atmosphere, followed by 30 seconds in reducing Ar(90%) and H_2(10%) to further remove the oxide residuals from the surface. The actual growth of graphene is carried at 1000 °C for 300 seconds in a mixed atmosphere of Ar(80%), H_2(10%) and CH_4(10%) in which the high temperature is used to decompose the methane molecule and create carbon radicals that react with the substrate and nucleate on its surface due to the catalytic properties of copper. The system is then cooled as

[1] GoodFellow PT000248, 50 µm, purity 99,95%
[2] GoodFellow, 25 µm, purity 99,9%

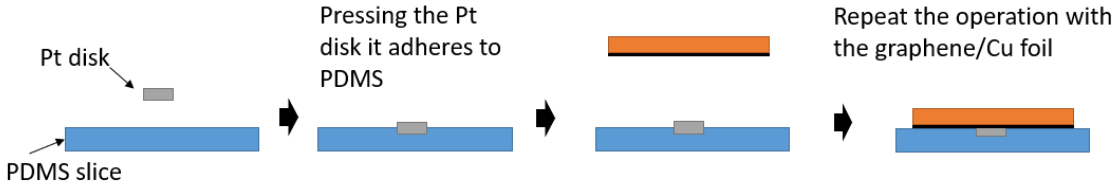

FIGURE 3.1: Transfer process of single layer graphene on platinum electrodes.

fast as possible to 200 °C in Ar(90%) and H_2(10%) and then to room temperature in inert argon atmosphere.

The grown layer is a single sheet of carbon atoms that can be transferred to the desired substrate. The platinum disks are first placed onto a polydimethylsiloxane (PDMS) slice with the top-side facing upwards. The graphene-copper foil is pressed onto the PDMS in the same way, as shown in figure 3.1, with the graphene side facing toward the platinum disk.

The whole system is then put in iron chloride ($FeCl_3$) solution to etch the copper film for 30 minutes at ambient temperature. When the copper is completely removed, the system is rinsed three times in deionized water for 15 min, in order to remove all $FeCl_3$, Cu and iron oxide residuals.

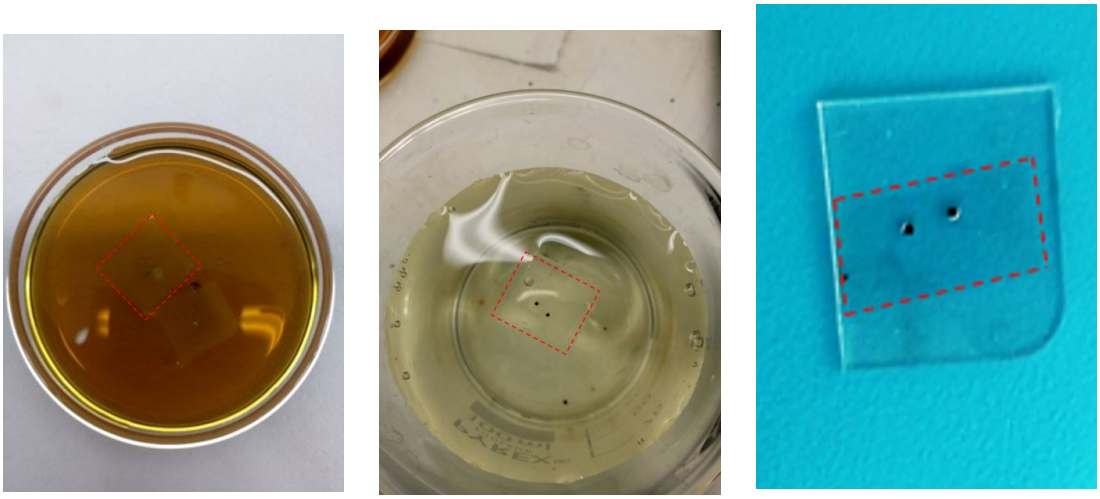

(A) Copper etchant. (B) Rinsing in water. (C) SLG film on Pt-disks and PDMS.

FIGURE 3.2: Transfer process of single layer graphene on platinum electrodes.

In order to check the presence and the quality of the transferred graphene layer present on the surface of the disks, the most commonly employed technique is Raman spectroscopy. Graphene layers cannot be seen under an optical microscope on most substrates, i.e. copper, therefore a different technique has to be employed. In order to be able to see and determine the number of graphene layers with an optical microscope, a 300 nm film of silicon dioxide is necessary. As instead, atomic force microscopy (AFM) has been longly used to identify single and few layers, but the throughput is low and the

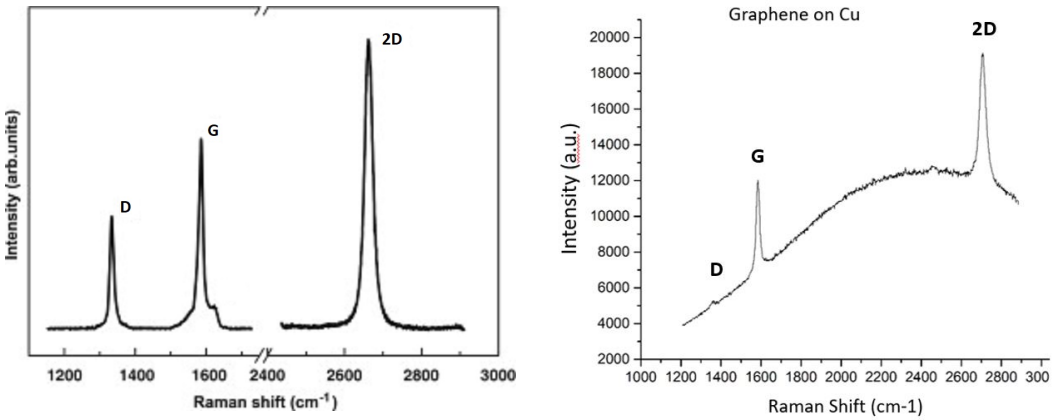

(A) Typical behavior [40].

(B) Measured spectrum

FIGURE 3.3: Comparison between typical spectrum of SLG and that measured on copper film before the transfer process.

resolution is not possible to distinguish between one and two layers, therefore a different technique has to be employed. Moreover, AFM is only be used on highly-oriented pyrolitic graphite, which has a completely flat surface at the atomic level, and therefore AFM cannot be used on the native copper film or the PDMS layer after the transfer process because they are not rigid enough. Raman scattering is a powerful light scattering technique that can be employed to analyze and investigate the internal structure of molecules and crystals. The source of irradiation is a laser beam of known frequency and polarization, which is scattered by the sample and a frequency shifted radiation is collected and analyzed. Raman scattering involves the creation and destruction of an optical phonon, which causes a shift in the frequency of the scattered radiation. The "Raman shift", i.e. the frequency difference between the incoming and scattered photons, is independent on the excitation frequency, therefore it is an intrinsic property of the sample. The unique electronic structure of graphene is reflected in its Raman spectrum and since it changes between single layer, bilayers and few layers, those differences can be detected with a high-throughput, non-destructive measurement.

The Raman spectrum, shown in figure 3.3, is characterized by a G peak at roughly $1580\,\mathrm{cm}^{-1}$ and a 2D peak around $2700\,\mathrm{cm}^{-1}$, given the first by the vibration of sp^2 hybridized carbon atoms in an hexagonal plane, and the latter is given by second order zone-boundary phonons, [19]. The D peak, located at $1360\,\mathrm{cm}^{-1}$, is produced by defects in the crystal structure of graphene. It can be observed in graphite and ideally it should not be present in a single-layer graphene Raman spectrum. 2D peak is the main one in mono-layer graphene and it broadens as the number of layers is increased.

Raman spectroscopy was performed on the platinum disks with transferred graphene in order to evaluate the quality of the graphene and the degree of coating of the metallic surface, through Renishaw inVia Reflex apparatus and an excitation laser source at 514.5 nm. Figure 3.4 shows that the transferred graphene did not provide a uniform and continuous coating of the underlying metal. Left spectrum represents a high quality graphene layer with low D peak, corresponding to few defects, while the right one does

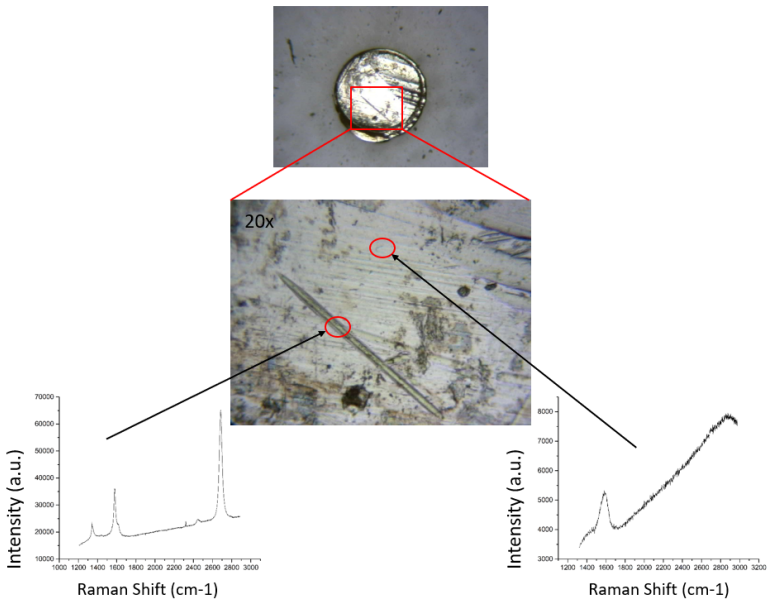

FIGURE 3.4: Comparison of Raman spectra of two different regions on a platinum disk.

not show the characteristic 2D peak. This may be due to the poor planarity of the surface which impaired a good transfer process from the copper foil to the disks placed on the PDMS sheet.

3.1.2 FLG growth

The growth of graphene can also be performed directly on platinum, without the use of copper as a catalytic substrate for the nucleation of graphene in the CVD process. The possibility of avoiding the presence of copper in the fabrication process eliminates the risk of copper contamination of graphene, which can be a major problem in biological and medical applications. The etching of copper and the transfer of graphene to a different substrate always leaves residuals of copper on the side of graphene previously exposed to the copper foil. Moreover, in CVD processes at 1000 °C, Cu can partially evaporate and copper ions can contaminate also the top side of the graphene layer, as well as the CVD chamber, [42]. In addition, growing graphene directly on the platinum substrate that can be used for the electrode eliminates the need of the transfer step, which is one of the most critical and challenging steps of the whole fabrication process, as seen in the previous section.

The platinum foils were the same used in the previous section to obtain the disk electrodes. After cleaning in acetone and drying in nitrogen flow to eliminate contaminants from the surface, the foils were inserted in the reaction chamber of the same CVD apparatus and annealed for 10 minutes at 1000 °C in N_2 flow to increase the crystallinity of the platinum surface. In figure 3.5 it is possible to see the effects of thermal annealing on the

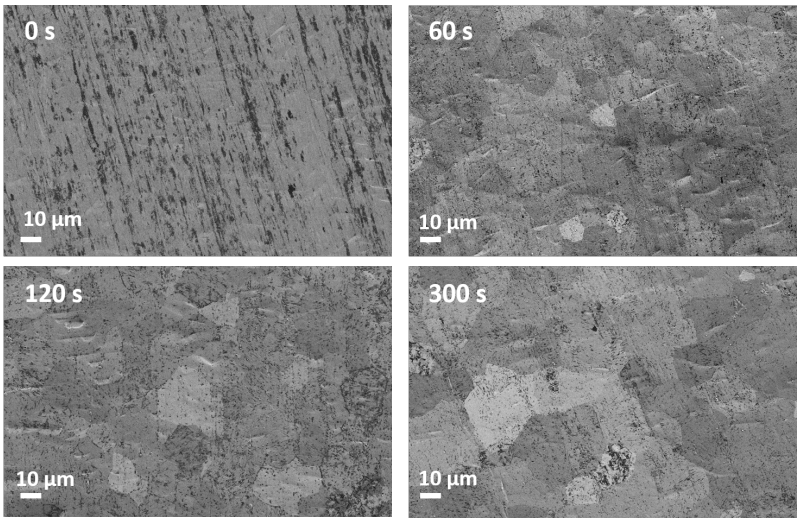

FIGURE 3.5: FESEM images of platinum foils at different growth times: [0, 60, 120, 300] s. (SE2 detector)

platinum foils. In the image at zero seconds it is not possible to observe crystalline feature, whilst in the three following images, it's possible to see the effects of thermal treatment, producing a polycrystalline structure on the surface. In these low-magnification pictures it is not possible to observe any presence of graphene.

The steps following thermal annealing are the same as the growth on copper film, with a pre-treatment in Ar and H_2 to further remove contaminants and growth at 1000 °C with methane. Various growth times were tested in order to evaluate parameters that produced the best quality graphene: 120 and 300 seconds of deposition time gave rise to a high quality graphene, as shown by the Raman spectra of figure 3.6.

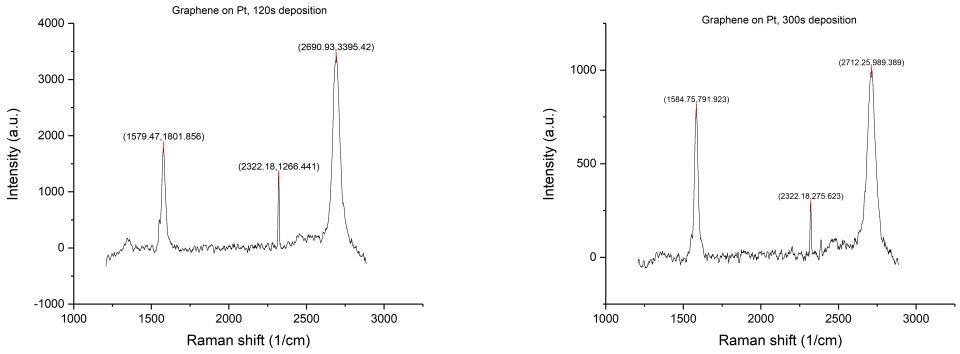

(A) 120 seconds (B) 300 seconds

FIGURE 3.6: Raman spectra at different deposition times of graphene grown on platinum.

The quality of the obtained graphene is comparable between the 300 and the 120 seconds, therefore in the following electrochemical measurements the samples grown for 300 seconds will be used. The presence of graphene on the platinum surface was investigated also with scanning electron microscopy. With a higher magnification, using in-lens

detector to enhance the morphology, it is possible to see the boundaries of platinum crystals, large regions with different shades of gray, and features that denote the presence of graphene 3.7a. Wrinkles are the main indicator of a graphene layer, especially when they cross the edge of a platinum grain 3.7b. The darker areas, as well as the black spots, may denote the presence of multilayers, as observed by Nam et al., the solubility of carbon on platinum surface at growing temperatures (1000 °C) is not negligible and it may cause carbon segregation and small multilayer regions underneath the continuous graphene film, [42].

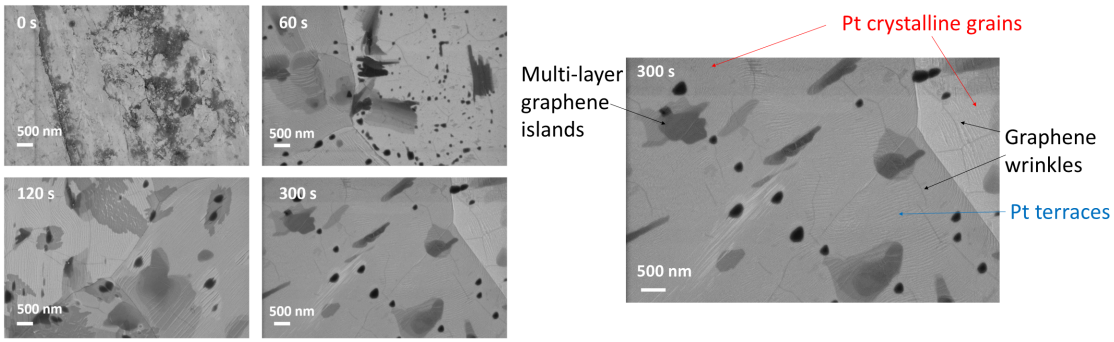

(A) Intermediate magnification (B) 300 seconds

FIGURE 3.7: Fesem images of graphene on platinum at different growing times with observable graphene features.

The foils have then been cut into smaller pieces to obtain samples with the right dimensions for the testing, roughly 5x12 mm.

3.1.3 LIG

The second class of electrodes is not based on a metallic substrate, which provides great advantages in terms of flexibility and mechanical properties. The LIG 3D structures are directly written through laser irradiation of a polymeric substrate: it is a single step process which allows great flexibility and versatility in shape and properties of the obtained structure. The substrate used to produce the laser induced graphene layer is commercially available polyimide film irradiated with a nanosecond CO_2 laser, controlled by a micromachining system by Microla Optoelectronics srl with tunable power, frequency and scan speed. Studies by Lamberti et al. showed that changing the scan speed and the frequency of the laser, structures with different properties could be made, defined *sheets*, *needles* and *porous* depending on the different morphologies observed at FESEM [34]. For applications in the neurostimulation field, one key parameter is the electrochemical behavior and a frequency of 4 kHz and scan rate at 160 mms^{-1} produced the needle-like structure of figure 3.9 with lowest electrochemical impedance and highest specific capacitance among all LIG tested, as shown by figure 3.8.

Scanning electron microscopy images of the graphitized area show that the underlying PI layer is not affected and the film maintains its structural stability, providing a stable substrate to the porous carbonaceous structure. Raman spectroscopy of the LIG

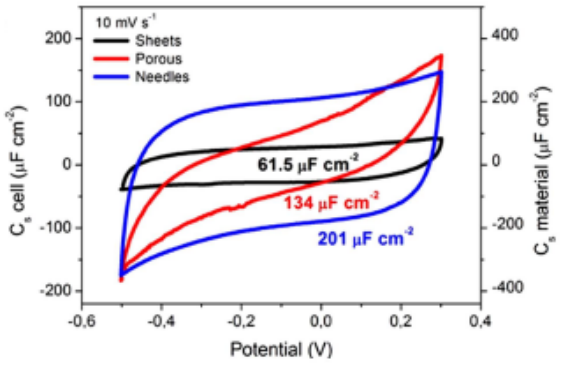

FIGURE 3.8: Comparison of cyclic voltammetries results for different LIG morphologies [34].

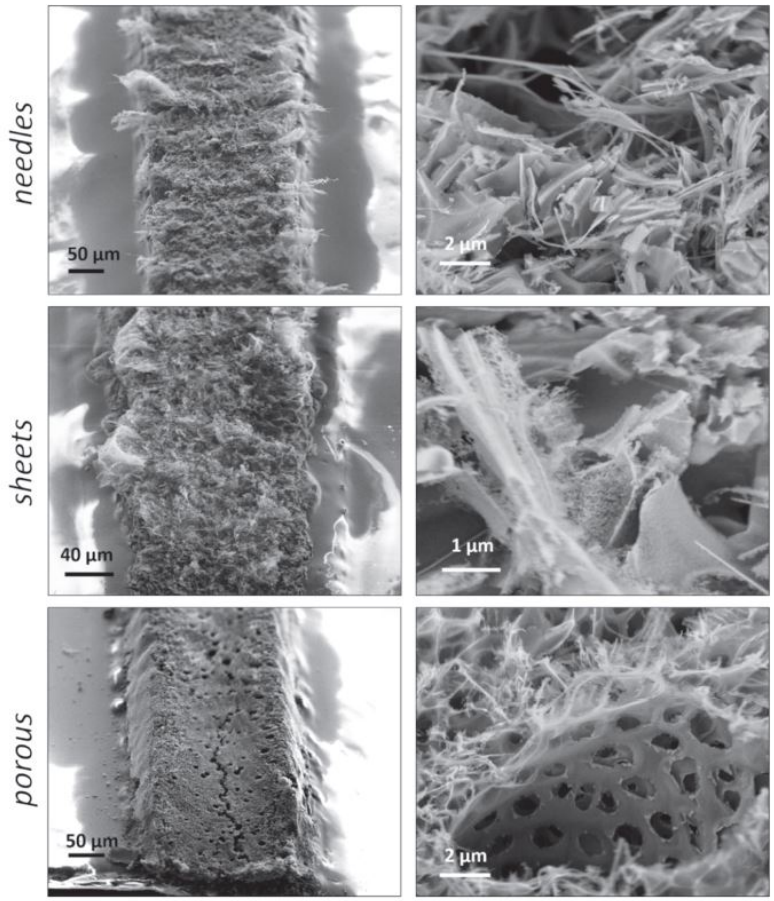

FIGURE 3.9: Low and high magnification FESEM images of LIG samples, [34].

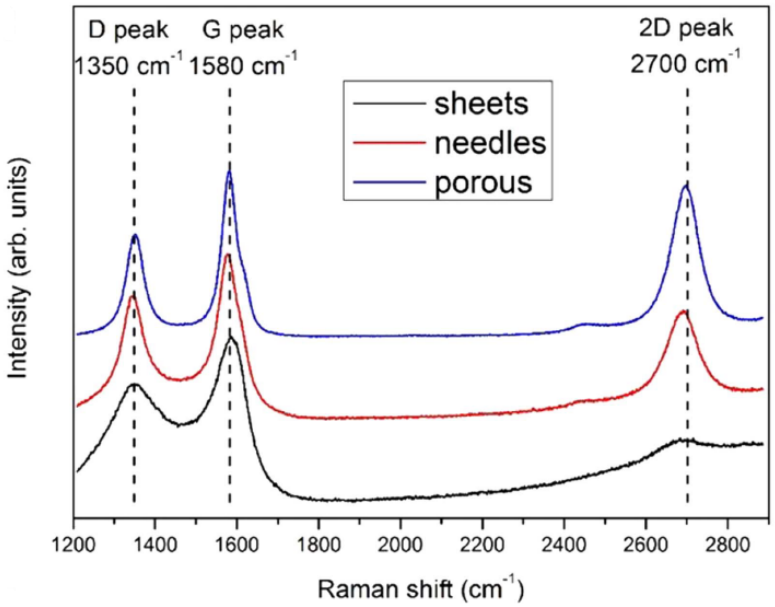

FIGURE 3.10: Raman spectrum of LIG samples with different morphology, [34].

samples have been performed, showing a spectrum typical of multi-layered graphene, with a D band at $\sim$1350 cm^{-1}, given by defects, vacancies and non-planar sp^2 bonds, and the typical G and 2D band at $\sim$1580 cm^{-1} and $\sim$2700 cm^{-1} respectively 3.10. The *sheets* and *needles* structures have similar raman spectra, while the *porous* LIG has a much less evident characteristic 2D peak.

The porous network of graphene can be subsequently transferred to an elastomeric substrate such as PDMS that ensures good transparency, elasticity and most importantly it has been widely used in biomedical applications due to its biocompatibility and stability in biological environments. Medical grade silicone is poured on the Kapton film and placed into low vacuum chamber to allow degassing of air bubbles that may have been entrapped in the silicone, allowing for a better penetration of the graphene flakes into the uncured PDMS. It is then fully cured [3] to allow the complete reticulation of the silicone structure that will embed the conductive LIG structures. The cured silicone sheet is then manually peeled from the PI film, obtaining a material with the mechanical properties of the elastomer and the good conductivity and high surface area of the LIG structures.

Song et al. improved the electrochemical properties of LIG electrodes by doping with PEDOT which is known for its good electrical conductivity and biocompatibility [49]. The LIG samples, prior to transfer to the PDMS substrate, are dip-coated with PEDOT aqueous solution, by repeated submersion and drying cycles to ensure a deep penetration of the conductive polymer within the three dimensional graphene structure. The transfer process to the silicon substrate is the same as the undoped samples.

[3] transferring recipe still to be determined. All attempts were unsuccessful.

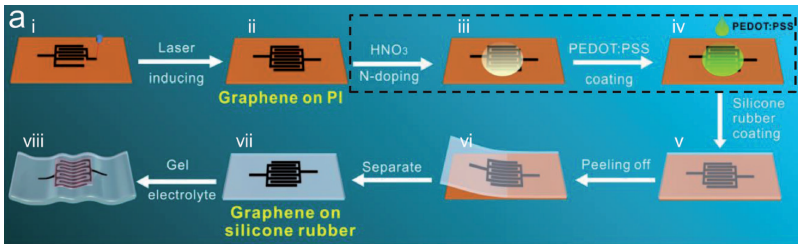

FIGURE 3.11: Process sequence of LIG electrodes: writing, doping, PDMS coating and peeling, transferred LIG electrodes [49].

3.2 Design of testing chamber

All electrochemical measurements have been performed in a custom made testing chamber that would allow for repeatable measurements with stable conditions among all types of electrodes. The apparatus features a metallic base that connects the working electrode to the external circuitry and a plastic part that controls the area of the working electrode exposed to the electrolyte, it also contains the electrolyte and the counter and reference electrodes. All measurements use phosphate-buffered saline (PBS) as the electrolyte, since it can mimic the properties of the physiological fluid found in biological environments.
The base is a 9 mm brass plate, milled to obtain a flat surface with 4 alignment posts and 2 threaded holes for screws, as shown in figure 3.12.

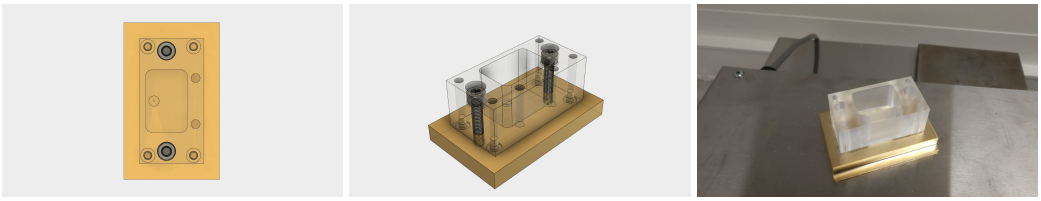

(A) Top view (B) 3D rendering of chamber (C) Picture

FIGURE 3.12: CAD images and real picture of the testing chamber.

The actual chamber is obtained from a 25 mm thick acrylic block that has been milled to realize the container for the solution, the holes for the reference and the counter electrodes, as well as the holes for alignment and screws. Once milled, the bottom wall of the chamber was 2 mm thick: drilling a hole of submillimetric diameter directly through the base would not guarantee a good transport of solution and a high risk of trapping air. Therefore a preliminary partial hole has been drilled with a 5 mm drill-bit to create a conical cavity. In its center a 400 µm hole has been drilled, with a length approximately of 0,5 mm, that defined the area of the electrode actually exposed to the electrolyte.

To guarantee a leakage-proof sealing, an O-Ring made from a thin silicone film has been glued to the bottom side of the acrylic chamber. A 50 µm thick medical grade silicone was glued with low viscosity silicone glue[4] to the bottom of the PMMA chamber

[4]Permatex flowable Silicone Windshield and Glass sealer.

and let cure overnight.

All chosen materials are highly transparent which is a great advantage in the placement and alignment of the samples in the testing apparatus, allowing for a direct optical control of the position of the sample electrode along all assembling steps.

The milling has been performed with Roland MDX-540 benchtop milling machine, both for the acrylic and the brass, controlled by a CAD model.

3.2.1 Electrochemical three-electrodes cell

The system described before is created to evaluate the electrochemical properties of the different sample electrodes, in processes that involve the transport of charge across the interface between the electrode, an electronic conductor, and the electrolyte, which is an ionic conductor. The electrochemical cell that provides the best and most reliable measurements is based on a three-electrode configuration composed by

- a working electrode;
- a counter (or auxiliary) electrode;
- a reference electrode.

The working electrode is the terminal of the cell of which we are interested in knowing the properties, such as the potential, which must be referred to a reference electrode that has stable and constant composition and potential [4]. The primary reference electrode, accepted internationally, is the *standard hydrogen electrode*, but for experimental reasons, other reference electrodes are often employed, for example, the silver-silver chloride (Ag | AgCl) reference electrode. The Ag | AgCl electrode has a constant composition and it is based on the equilibrium of the redox reaction between the silver metal and the silver-chloride salt. Its potential is fixed and it is 0.222 V with respect to the standard hydrogen electrode. The Ag | AgCl electrode[5] used in our cell has silver wire coated with silver-chloride inserted into a 4 mm glass tube filled with 1M KCL solution, with a porous Teflon plug that allows interaction with the sample electrolyte. It is kept in 1M KCl solution when not used for testing to ensure stability of the potential, given by the concentration of chloride ions in the glass tube, since its potential is related to the concentration of Cl^- by the Nernst equation.

The counter electrode is the current carrying one and it is made by a platinum foil with large surface area exposed to the electrolyte. In our case it is a 25 µm thick, 2 mm wide and 20 mm long platinum foil, which does not react with the electrolyte producing species that may interfere with the working electrode. Its area is at least 100 times larger than the working electrode exposed area.

[5] CH Instruments, Inc. CHI111 Ag | AgCl reference electrode.

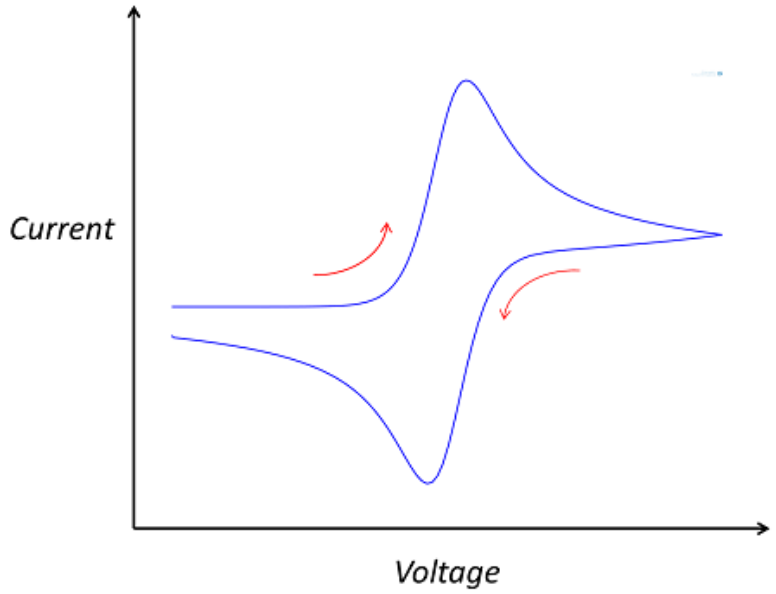

FIGURE 3.13: Generic cyclic voltammogram with the current response to the driving applied voltage [41].

3.3 Electrochemical Measurements

The most common techniques to characterize electrodes for neural applications are cyclic voltammetry and electrochemical impedance spectroscopy, since they can be employed both in vitro and in vivo with minor differences, allowing for a comparison of performances of the same electrode. In the present work all techniques have been employed only in vitro with the experimental setup described before.

3.3.1 Cyclic Voltammetry

Cyclic voltammetry (CV) is an electrochemical measurement in which the potential of the working electrode is linearly swept between two limits at a constant rate.

The experiment can be performed with different setups: with a two or a three-electrode cell, according to the necessities and the limitations of the measured system. In the present case the measurements are carried out in a three-electrode cell that ensures the most reliable results. The potential of the active electrode is referred to the non current carrying Ag | AgCl electrode and forces a current to flow between the working electrode and the platinum counter electrode. Reactions are driven by the potential at the test electrode, while the current represents the rate of the occurring reactions. The CV provides information on the presence of electrochemical reactions, their reversibility, the quantity of electroactive material and its stability under stimulation [12].

The main parameters that affect the voltammogram are the sweep rate and the potential window, that can be directly controlled, the geometric area, which in the present case is kept constant, and roughness of the surface, that depends on the kind of material

tested. At the interface between the electrode and the electrolyte, at low intensity, injection of charge is dominated by capacitive mechanisms and double-layer formation, which is ideally desirable because no chemical species are formed. At higher intensities, first, reversible Faradaic reactions take place, such as oxidation and reduction, hydrogen plating and stripping. Ultimately, further increasing the intensity, the process is dominated by irreversible reactions, such as electrode corrosion, water electrolysis and chlorine ions oxidation.

The potential limits are chosen in order to prevent water hydrolysis, since all experiments are carried out in PBS, which could lead to formation of hydrogen ions and hydroxyl groups that are highly reactive and would change the pH of the solution. It has been long documented that pH changes can have significantly interfere with the cell functions, such as enzyme activity modulation and changes in the ionic conductance of the cell membrane, and large pH changes can lead to necrosis [30].

For platinum the water window is known to be between -0,6 V and 0,8 V, therefore all CVs are carried within those limits. The other directly controllable electrical parameter is the sweep rate: the voltammogram depends on many parameters, but in the present case it is the only one that can be freely chosen, since the water window is fixed and the exposed area determined by the geometry of the experimental chamber. A high sweep rate gives information on the exposed area of the electrode, while lower sweep rates include details also on the more occluded regions of the electrode, since a lower sweep rate allows the electrolyte to penetrate into the cavities of a porous structure. In this study all cyclic voltammetries are performed at $150\,\mathrm{mVs}^{-1}$, so that performances of different electrodes can be directly compared, having been tested all in the same conditions.

The charge storage capacity (CSC) is a measure of the total charge that can be stored in the electrode for each stimulation pulse and it is calculated as the time integral of the cathodic current over the potential window: $CSC = \frac{1}{Area} \int |i(t)|dt$.

3.3.2 Electrochemical Impedance Spectroscopy

EIS is a measure of the impedance obtained stimulating the working electrode with a small sinusoidal voltage signal in a broad range of frequencies and measuring the current response of the system. The excitation voltage signal is given by a DC bias and an AC perturbation, which is small enough that linearity is preserved at all frequencies, figure 3.14.

The response of the system will be given by a current at the same frequency of the voltage excitation, with a phase shift given by the reactive components of the system's impedance, capacitive and inductive effects, figure 3.15.

Using the frequency-domain definition of the applied voltage and the measured current of equation 3.1, the impedance will be frequency dependent and it can be written as a complex number with real and imaginary part, equation 3.2.

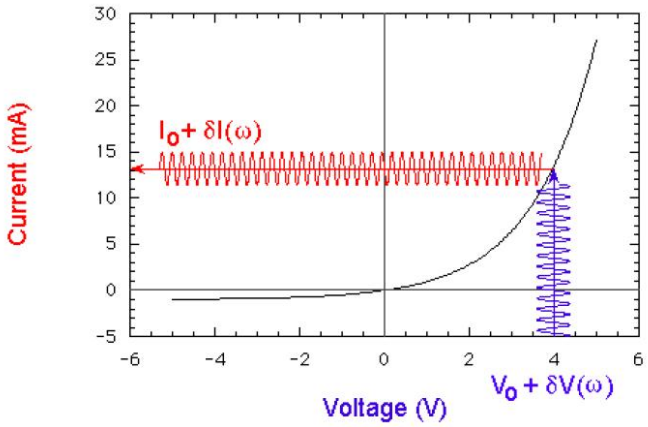

FIGURE 3.14: Small AC voltage perturbation and the consequent current response.

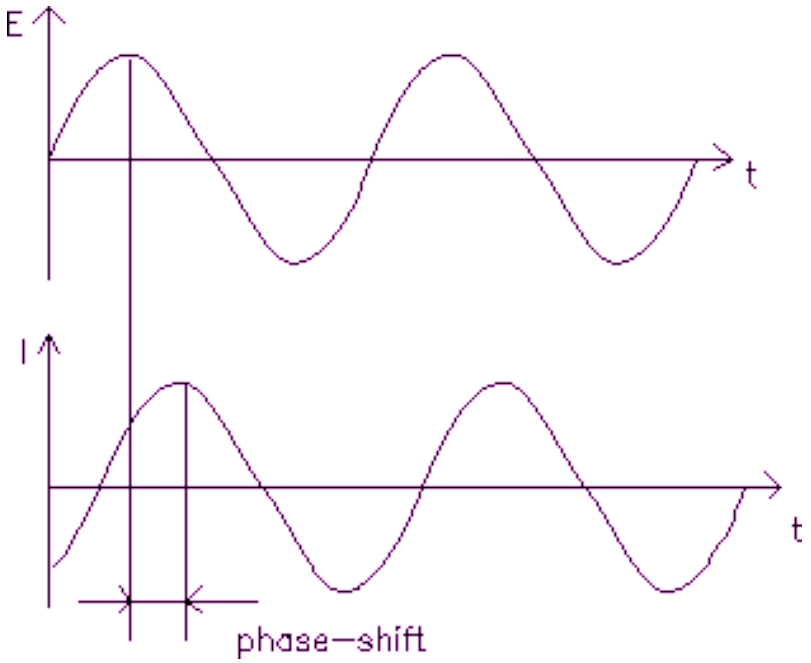

FIGURE 3.15: Time-dependent representation of excitation AC voltage and recorded AC current with focus on the frequency-shift.

$$\begin{cases} V = V_m e^{j\omega t} \\ I = I_m e^{j(\omega t - \phi)} \end{cases} \tag{3.1}$$

$$Z = \frac{V_m}{I_m} e^{j\phi} = \Re e\{z\} + \Im m\{z\} = z_1 + jz_2 \tag{3.2}$$

The spectrum of $Z(\omega)$ can be given as a projection onto the z_1-z_2 plane, which is called Nyquist Plot, or as a Bode plot: in this case the logarithm of modulus and phase are plotted as a function of the frequency in two different plots or superimposing them.

One of the most significant figures of merit is the impedance at 1 kHz. In the present case the bias voltage is set to zero, the alternating signal has an amplitude of 50 mV and the frequency is scanned between 1 Hz and 10^5 Hz through an impedance analyzer (Gamry 1000E) in the same three-electrode cell configuration described for the cyclic voltammetry.

3.3.3 Pulsed Stimulation

Voltage transients are a common technique to evaluate the maximum charge that can be injected by a stimulation electrode. The stimulation pulses are current controlled and the maximum polarization is measured using the sample as the active electrode and the same large platinum electrode used in cyclic voltammetry and electrochemical impedance spectroscopy as the return electrode. The current waveform is biphasic, symmetric cathodal-first squared pulse with a small interphase period between the cathodic and the anodic phases, in which the total charge is null since the anodic and cathodic charges are equal. It is used to determine E_{mc} which represents the maximum negative polarization of the electrode-electrolyte interface and consequently the Charge Injection Capacity (CIC) which is a measure of the maximum charge that can be injected from the electrode to the electrolyte.
In neural electrodes for stimulations, the CIC is evaluated as the cathodal current times the pulse width that drives E_{mc} to the most negative potential of the water window. The current and the pulse-width are independent parameters that can be adjusted in order to drive the electrode to its maximum polarization, before causing water electrolysis, i.e. E_{mc}=-0.6 V.

The current pulse is applied through a stimulation device to the working electrode and the voltage response is measured with a digital oscilloscope (Agilent MSO-X 3024A) to visualize the voltage pulse, the current is increased until E_{mc} reaches -0.6 V and the injected charge is evaluated as the current flowing through the electrode-electrolyte interface times the pulse width.

For LIG samples, since the water window is wider, current and pulse width are set in order to reach a lower E_{mc} equal to -1,2 V as shown in figure 3.16.

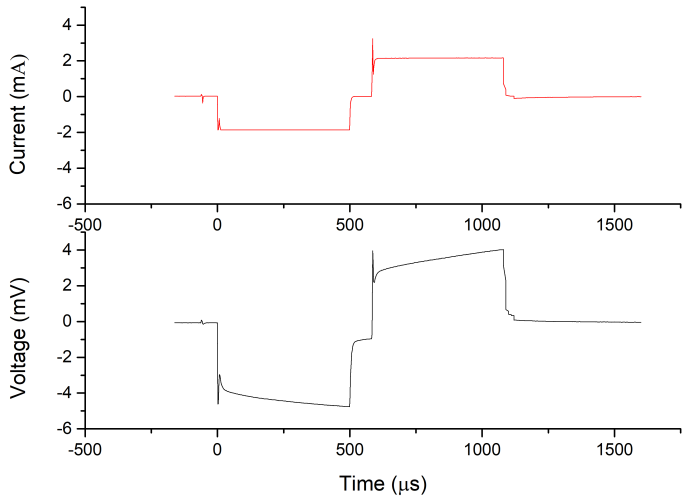

FIGURE 3.16: Current and voltage pulses with pulse width of 500 µs

.

3.3.4 Accelerated Aging

An accelerated aging test is conducted in order to evaluate the chemical and mechanical stability of the samples. It consists in keeping the sample in liquid at high temperatures, which simulates the long term aging in a living body, assuming that the variation in properties given by chemical reactions will be accelerated by increasing the reaction rate as a consequence of higher temperatures. The samples are kept in a PBS filled container and placed in an environmental chamber at 90.0 °C and tested once per week to evaluate the stability of the samples and the differences in electrochemical properties.

The aging is accelerated by keeping the system at a higher temperature than what it would get in standard conditions and it is evaluated through a formula that takes into account the difference in temperature and the material involved 3.3.

$$AAT = D_{RT} \cdot AAF = D_{RT} \cdot Q_{10}^{-\frac{T_{AA}-T_{RT}}{10}} \tag{3.3}$$

AAT represents the *Accelerated Aging Time* which is the time the sample spends in the environmental chamber, D_{RT} represents the *Desired Real Time*, which is the time it would take to age to the same degree at room temperature T_{RT}. On the contrary, T_{AA} is the *Temperature of Accelerated Aging* at which the environmental chamber is set. Q_{10} lastly is the aging coefficient which takes into account the material of the aged sample. Its value is constant for each material and it is retrieved from previous studies: it has long been known to range between 1.8 and 3 for polymeric materials. Since no values could be found for polyimide films, all calculations will be made considering the worst case scenario, i.e. the slowest aging coefficient 1.8. Therefore the equation used to evaluate the aging of the LIG samples is

$$AAT = D_{RT} \cdot AAF = D_{RT} \cdot 1.8^{-\frac{90-37}{10}} \tag{3.4}$$

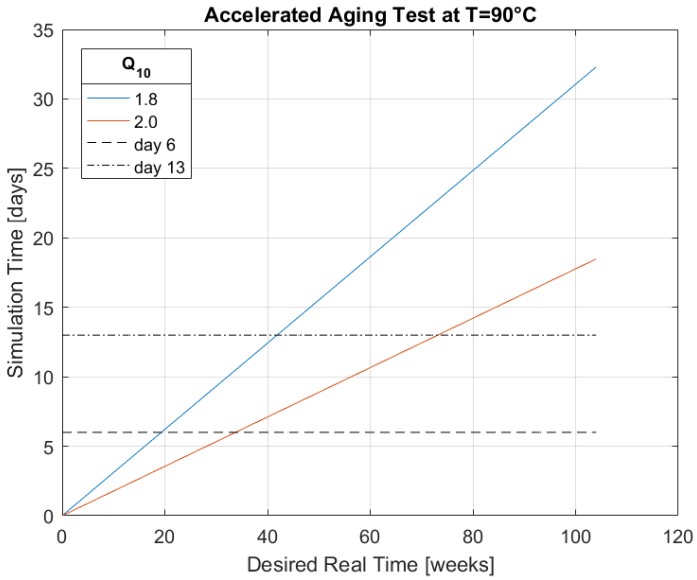

FIGURE 3.17: Simulation of accelerated aging at 90 °C with aging coefficients of 1,8 and 2,0.

Chapter 4

Electrochemical characterization

4.1 Electrochemical measurements

The electrochemical characterization has been performed in order to evaluate the electrochemical properties of the interface between the electrode, i.e., the tested sample, and the electrolyte, which represents the equivalent to the neural tissue or physiological environment in which the neural electrode would be employed.
All measurements have been performed in 0.1 M PBS solution with the measurement setup showed previously.

4.1.1 Cyclic Voltammetry

The results of the cyclic voltammetries for all the tested materials will be presented in this section. In order to be able to directly compare the obtained results for all the samples, the main parameters involved in the measure, i.e. the potential window within which the voltage is applied, the sweep rate, which is the constant rate of change of the applied potential, and the interfacial area of the electrode which is exposed to the electrolyte, are kept constant.

Platinum The first measurement was performed on platinum samples since it represents the most commonly employed material in implantable devices for neural applications. Therefore it has been used to determine a baseline and a reference for comparison with the graphene-based electrodes. The measurements on platinum have been conducted with the electrical configuration presented in section 3.2, as well as the subsequent measurements on graphene, in such a way that a direct comparison between the results could be made, minimizing the impact of unknown effects.
Three different types of platinum samples were tested, with different exposed area, in order to evaluate the best possible measurement of the charge storage capacity, measured as the time integral of the measured current divided by the exposed area of the electrode, i.e. $CSC = \frac{1}{Area} \int |i(t)|dt$

As it can be seen in figure 4.1, the voltammograms of platinum disks of 400 µm 700 µm and 1 mm have similar shape, typical of platinum, but different area within the curve, which represents the CSC in the IV plane.

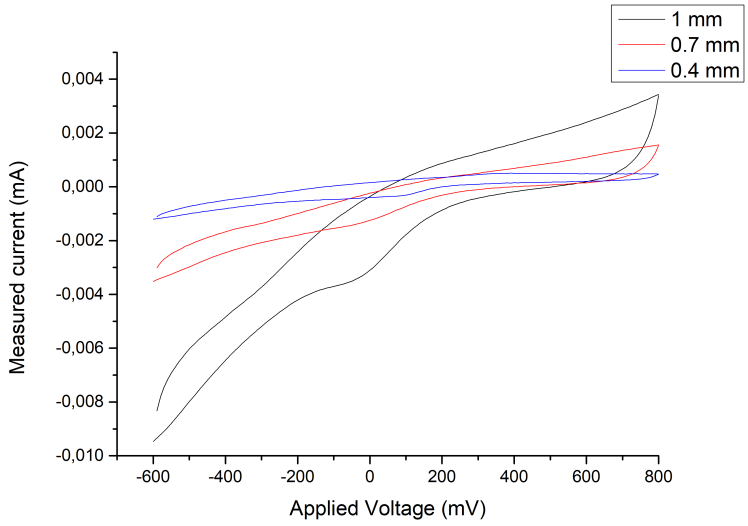

FIGURE 4.1: Comparison of CVs of platinum electrodes with different exposed area

However, if one considers the stored charge per unit area, as it can be seen in table 4.1, the values of CSC are relatively stable.

Single layer graphene and few layers graphene Once a solid reference of charge storage capacity for platinum has been obtained, electrodes coated with graphene have been tested. Firstly the electrodes coated with single and few layers graphene have been tested, in order to evaluate the change in surface properties of the coating. As shown in the section devoted to the fabrication of SLG and FLG electrodes, these electrodes consist of platinum coated with a two-dimensional graphene sheet.
In this set of measurements, the exposed area was always kept to a circle with a diameter of 400 µm, which is equivalent to 1.20×10^{-3} cm^2.

As it can be seen in figure 4.2, the voltammograms for SLG and FLG show a much worse behavior if compared to a platinum electrode of the same size.

For single layer graphene electrodes transferred from the copper foil to the platinum electrode, the worsening of performances could be due to the uneven coating of the metallic surface by the graphene film. As it has been shown in figure 3.4, during the transfer process from copper to platinum the graphene did not maintain its structural integrity and left regions of the underlying platinum surface exposed. Therefore the measurement of the SLG electrode could be seen as platinum with carbonaceous residues on its surface.

Laser induced graphene The last type of electrode that has been tested is the LIG on Kapton, since all the attempts of transferring the LIG to the PDMS have been unsuccessful. Since the porous graphene structures are directly written on the Kapton film, the brass base of the testing chamber, previously used as the contact to the back of the tested electrode, is not anymore in contact with the conductive graphene structures. Therefore,

TABLE 4.1: Results for Pt CVs at different areas

Diameter	400 µm	700 µm	1 mm
Area (cm^{-2})	$1,25710^{-3}$	$3,84810^{-3}$	$7,85410^{-3}$
	CSC (mC cm^{-2})	CSC (mC cm^{-2})	CSC (mC cm^{-2})
	1,648	3,141	4,407
	3,659	2,810	2,457
	2,357	3,833	2,564
	1,887	3,004	2,993
	1,399	1,937	2,398
	34,560	4,531	4,092
	2,435	5,418	2,731
	3,259	5,503	4,789
	4,741	5,323	3,805
		4,501	4,256
			4,739
			5,165

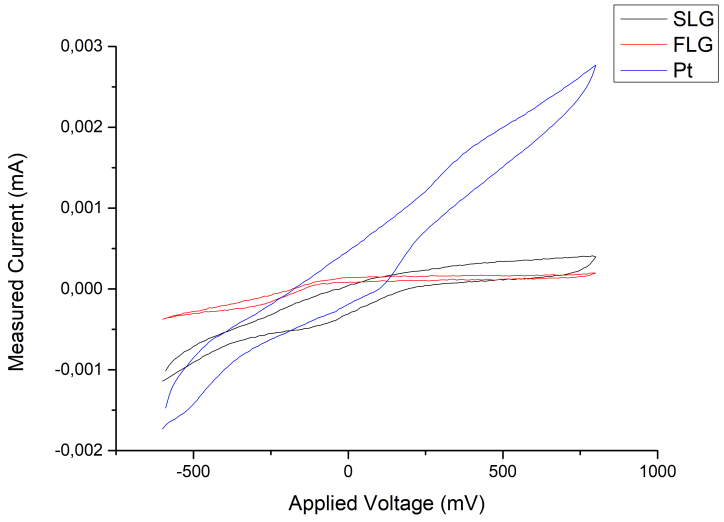

FIGURE 4.2: Comparison of single layer graphene, few layers graphene and platinum electrodes' voltammograms.

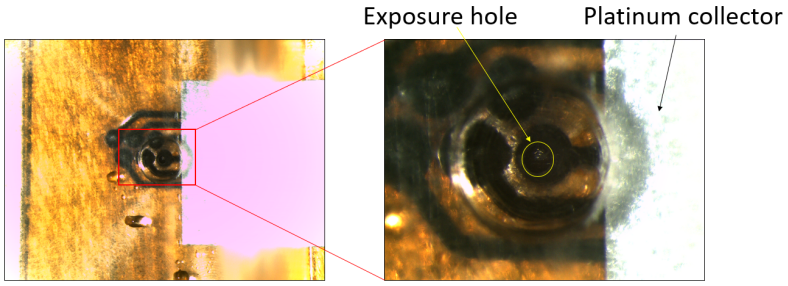

FIGURE 4.3: Picture of LIG electrode with inset on the exposure hole and platinum collector.

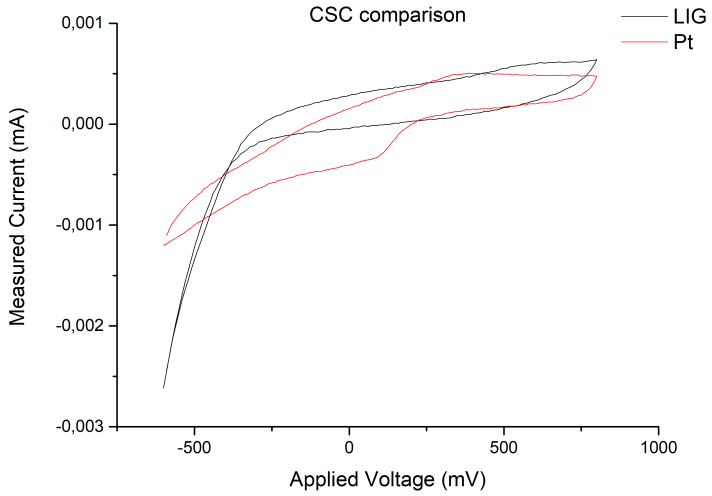

FIGURE 4.4: Comparison of CV curves for LIG and platinum electrodes.

in order to bring the signal to the LIG electrodes, a 50 µm platinum foil is used to contact the LIG electrode with the external driving electronics, simply by pressure contact between the platinum and the LIG, figure 4.3.

Previously to the electrochemical evaluation of the properties of the LIG, samples underwent a cleaning protocol to ensure that all fabrication residuals and unwanted chemical species were actively removed from the active surface of the electrode. It consisted in slower sweep rate cyclic voltammetries, i.e. $100\,\mathrm{mV\,s^{-1}}$, with a potential window of (-1,1) V for 20 cycles. Afterwards the parameters for the CV were set again to the ones used previously for platinum electrodes, and the voltammogram for LIG samples has been calculated. As it can be seen in figure 4.4, in which typical results for LIG and Pt electrodes are plot, even though the shape of the two curves is quite different, due to the differences in chemical composition of the two electrodes, the area within the curve, which represents the CSC, is comparable.

Subsequently a customized activation protocol was designed in order to evaluate the true maximal potential performances of the previously measured LIG electrodes. Samples were forced to perform cyclic voltammetries in a wider potential window, measured

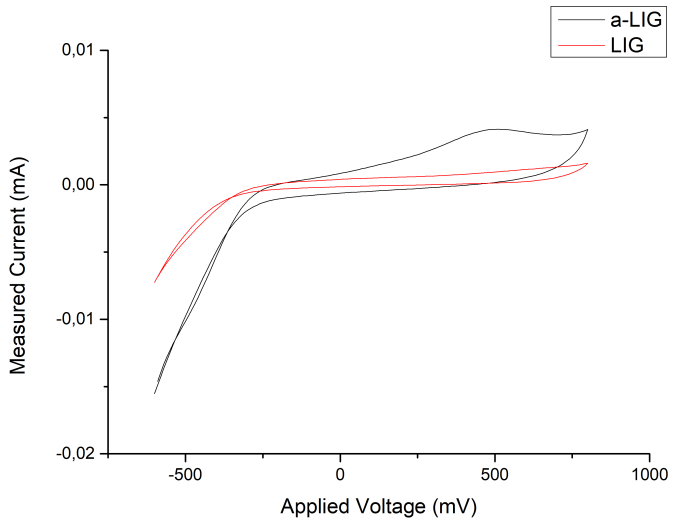

FIGURE 4.5: Comparison between CVs of LIG before and after activation.

in order not to exceed the water hydrolysis potential values. Increasing the potential window to (-1.4,1.2) V, the residual irreversible chemical reactions that were not consumed on the surface of the LIG structures, were forced to occur [14]. During the activation process, we suppose that the effective porosity of the LIG electrodes has increased. By increasing the potential with the same scan rate, the solution was able to penetrate more deeply in the pores, increasing the accumulation and storage of charges, such as hydrogen ions, more easily accessible in the subsequent cycles. A similar approach is typically used in supercapacitor applications, in which the conditioning of the system allows for a wider potential window and greater charge storage capacity [55].
After 10 activation cycles, the parameters were set again to those used for platinum and before the activation, in order to be able to make comparison between measurements performed in the same configuration and evaluation the differences between materials only.

In figure 4.6, it is possible to appreciate the comparison between platinum and LIG samples, before and after the activation protocol. As it can be seen, simply by cycling the samples at a wider potential allows for a significant increase in charge storage capacity of approximatively one order of magnitude.

After the measurements of the activated LIG samples, an accelerated aging protocol was started, placing the activated LIG array in PBS at 90 °C as explained in section 3.3.4. The array has been tested again, in the same conditions as prior and after the activation, after 6 and 13 days of aging in the environmental chamber in order to evaluate the eventual decrease in performances with time. After rinsing the samples in clean PBS, cyclic voltammetry was performed, evaluating the charge storage capacity of the LIG electrodes, without performing the activation cycles again. As it can be seen in figure 4.7, which shows typical results of a LIG electrode, the charge storage capacity of such

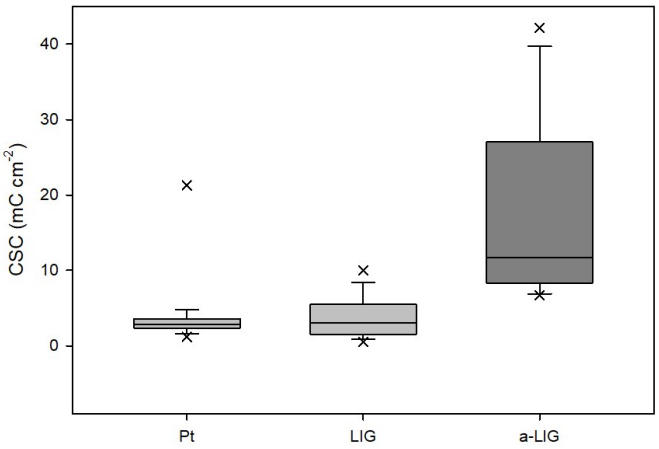

FIGURE 4.6: Comparison of CSC values for platinum, LIG and activated-LIG.

electrodes upon accelerated aging witnesses a minor decrease if compared to freshly activated electrodes.

The plot of figure 4.8 compares the CSC measurements for each electrode kind: first the platinum and the LIG before activation, and then the activated LIG electrodes at day 0 and after one and two weeks.

The results show a good stability of the charge storage capacity of activated LIG electrodes after aging, especially if compared to unactivated LIG and bare platinum which represents the clinical standard for implantable devices and did not show any sign of properties changing throughout the accelerated aging process. In both cases activated LIG holds the CSC at least one order of magnitude higher than platinum and unactivated LIG. Two weeks of accelerated aging are equivalent to approximately 40 weeks of aging at body temperature of 37 °C with the lowest aging coefficient Q_{10}=1.8, which means roughly one year in a living body, as can be seen in figure 3.17.

4.1.2 Electrochemical Impedance Spectroscopy

The second characterization technique employed to evaluate the properties of the electrode-electrolyte interface is EIS, in which the frequency-dependent impedance is evaluated by means of a small sinusoidal signal and recording the system's response. As for cyclic voltammetry, shown in the previous section, all electrode types have been tested in order to measure the electrochemical impedance and a comparison between the standard, platinum, and graphene-based electrodes have been made.
The most relevant parameter, as explained before, is the modulus of the impedance at 1 kHz frequency, since stimulation in vivo is usually performed in a range of frequency close to 1 kHz.

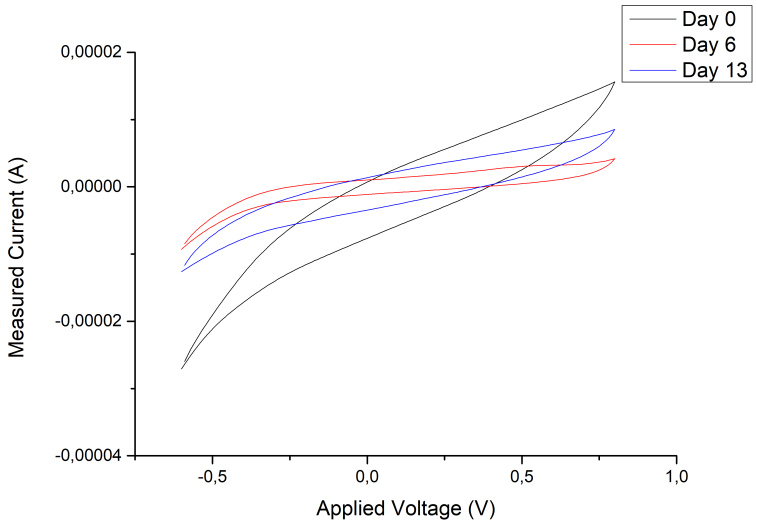

FIGURE 4.7: Comparison of CV curves of a LIG electrode at day 0, day 6 and day 13 of accelerated aging protocol.

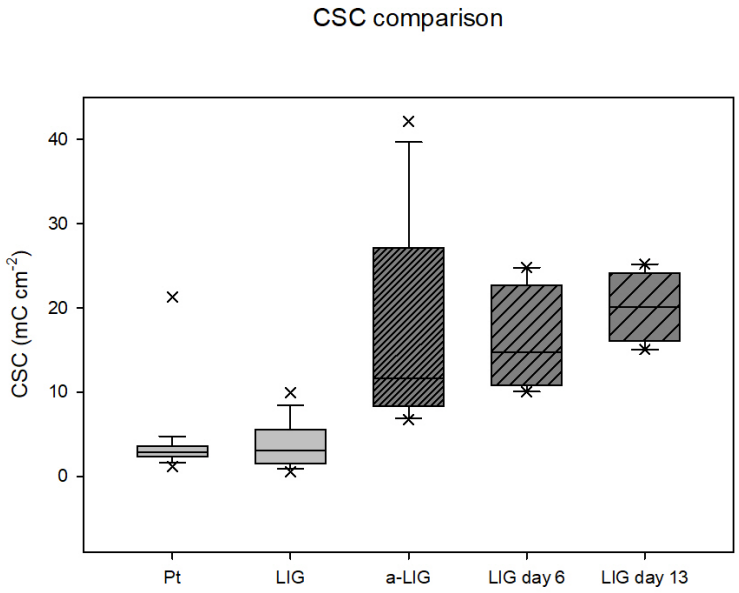

FIGURE 4.8: Comparison of aged LIG samples with platinum and unactivated LIG.

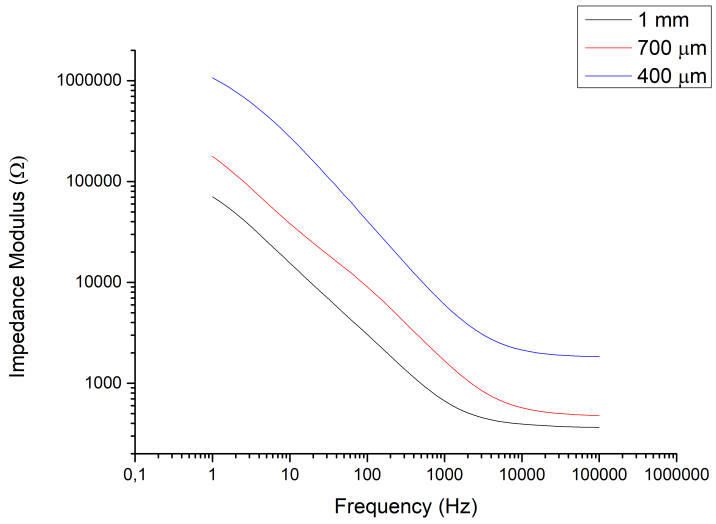

FIGURE 4.9: Comparison of EIS modulus for different sizes of platinum electrodes.

Platinum As before, platinum electrodes of different surface area have been tested, disk-shaped electrodes with diameter of 400 µm 700 µm 1 mm.

As shown in figure 4.9, the impedance, although with similar shape, has different values when changing the exposed area, increasing with the increase of diameter of the electrodes. Once again this behavior underlines the need of having a constant exposed area when evaluating the different materials for electrodes, in order to eliminate the dependence on the surface area. All sequent measurements will then be made with the same setup presented previously, with a 400 µm exposure hole and therefore a $1.20 \times 10^{-3}\,\mathrm{cm}^2$ exposed area, measured experimentally.

Single layer graphene and Few layers graphene The graphene-coated platinum electrodes have been measured to evaluate the electrochemical impedance, with the same three-electrode cell presented in the previous chapter, with a silver-silver chloride reference electrode and a large platinum counter electrode in PBS.
SLG and FLG show a different behavior for what concerns EIS, while SLG on platinum shows results quite similar to those of plain platinum, the impedance measured for electrodes coated with FLG is roughly one order of magnitude higher than platinum.

As shown in figure 4.10, the shape of all the curves is similar and SLG and platinum have a 1 kHz impedance almost equal, while the EIS for FLG-coated electrode is noticeably higher. As hypothesized previously, according to the Raman spectra of SLG electrodes, the transfer of graphene from the copper substrate to the platinum electrode produced a non-uniform coverage of the platinum surface, since the graphene sheet collapsed onto itself, leaving wide areas of the platinum surface exposed to the electrolyte, with few areas covered by carbonaceous residues, figure 3.4. This may be the cause

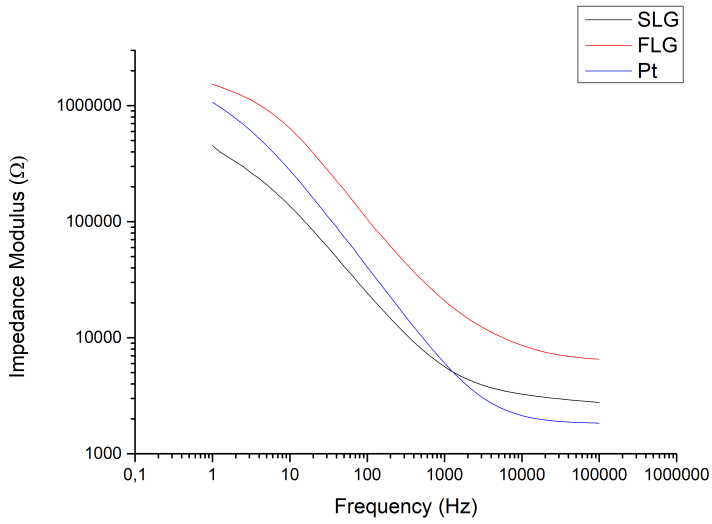

FIGURE 4.10: Comparison of EIS modulus between platinum and graphene-coated electrodes.

of the great similarity of properties for SLG and platinum, both concerning CSC and impedance.
For what concerns the few layers graphene structure instead, from the Raman spectroscopy it can be seen that the coating is much more uniform, with regions with single layer and other with few layers islands. As the charge storage capacity of has been measured to be much smaller than platinum, the impedance values are generally one order of magnitude higher than platinum and SLG, as it can be seen by figure 4.11, which compares the 1 kHz impedance modulus all measured samples for platinum, SLG, FLG and LIG electrodes.

Laser induced graphene The last material to be tested is LIG on polyimide: the experimental setup is kept constant as all previous EIS measurements and the LIG samples have been tested before and after activation and during the accelerated aging protocol. The setup is the same explained for the cyclic voltammetry, with the platinum collector placed as close as possible to the LIG electrode in order to minimize the resistive contribution of the LIG lines, image 4.3.

The impedance of LIG electrodes has the same pattern as platinum, see plot 4.9, and the activation of the material reduces the electrochemical impedance, as it increased the charge storage capacity. Figure 4.12 clearly shows the reduction of impedance modulus due to activation of the LIG and a slight increase during the accelerated aging protocol, both after one and two weeks.

Figure 4.13 compares all the tested LIG electrodes with platinum considering the most important parameter of an EIS spectrum, the modulus at 1 kHz. The synthesis of many different samples follows the same pattern as what shown in figure 4.12, with a noticeable reduction of impedance through activation, and a small increase during the accelerated

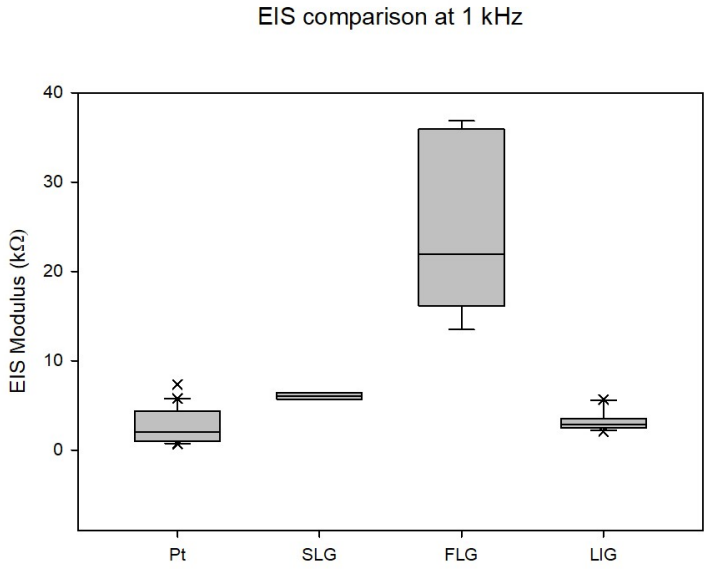

FIGURE 4.11: Comparison of EIS measurements for all four types of electrodes at 1 kHz.

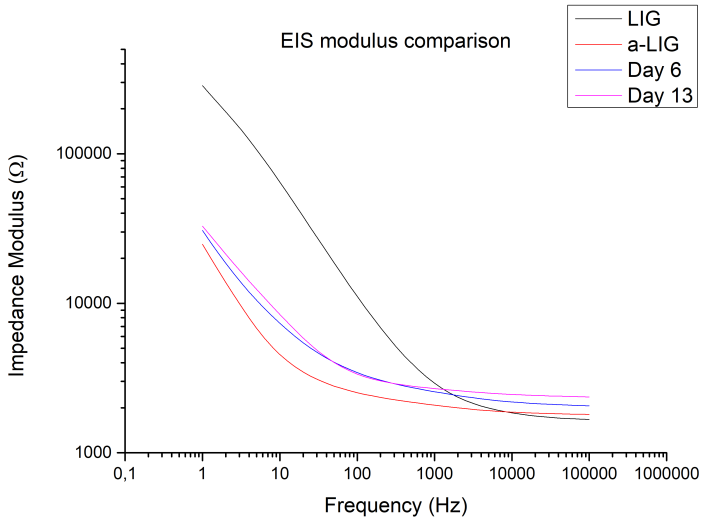

FIGURE 4.12: Comparison of EIS modulus for the same LIG electrode before and after activation and during accelerated aging.

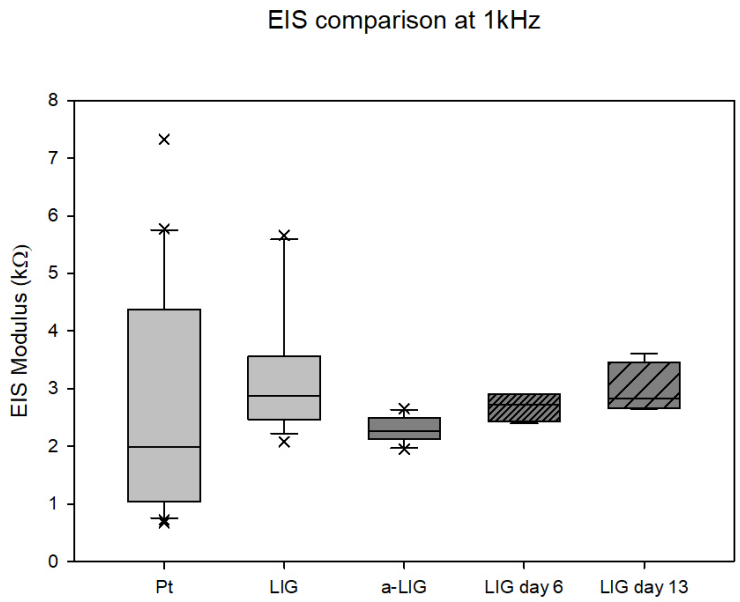

FIGURE 4.13: Comparison of EIS modulus between platinum, unactivated LIG and activated LIG at day 0, 6 and 13 of the aging protocol.

aging. However, even if slightly increasing, the impedance is still lower than unactivated LIG and comparable to the values of platinum.

After evaluating the impedance of the electrode-electrolyte interface, a new set of EIS measurements was performed, in order to evaluate the effects of the LIG tracks on the system's performances. The platinum collector, instead of being placed in the near proximity of the LIG electrode, has been moved further apart, as seen in picture 4.14, still leaving only the electrode's surface exposed to the electrolyte but adding a series resistance from the electrode to the platinum collector.

The increased distance of the metallic conductor from the exposed graphene electrode will induce a greater resistivity, causing a rigid vertical shift in the EIS spectrum. Figure 4.15 shows the increase in impedance of the LIG electrode when placing the platinum collector at a distance of 14 mm from the region exposed to the electrolyte.

The resistive contribution of the track only is calculated by subtracting the measured value of the impedance at 1 kHz of the LIG electrode only from the LIG+Track system. In order to calculate the linear resistivity of the LIG tracks, the resistance is then divided by the length of the track, allowing for a direct comparison with other conductors. The standard conductors chosen for the comparison are 50 µm diameter metallic wires: copper and platinum. This kind of leads is the most commonly employed in arrays of metallic electrodes. By dividing the resistivity of the metal, from literature [47], by the cross-section of the wire, the linear resistivity of the metals is retrieved.

- Copper: 7.55 Ω/m
- Platinum: 53.98 Ω/m
- LIG: 340.84 kΩ/m

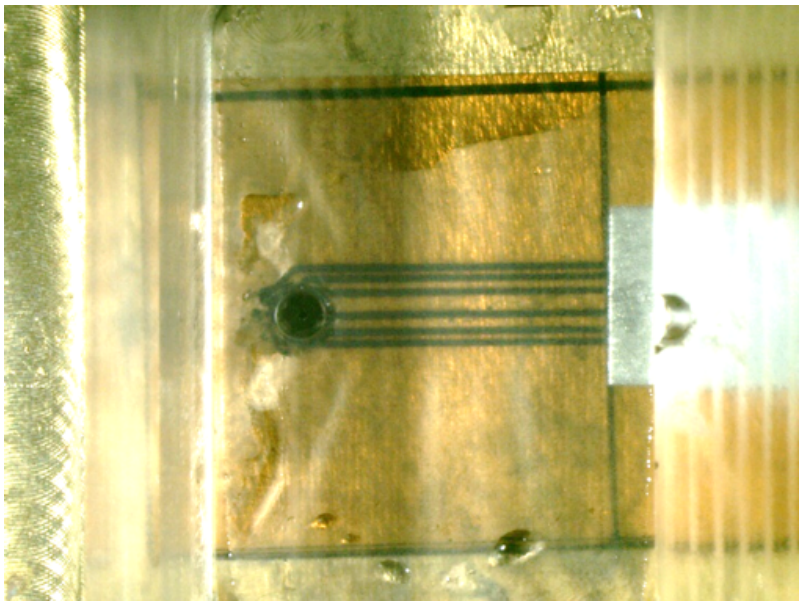

FIGURE 4.14: Placement of platinum collector with respect to LIG exposed electrode.

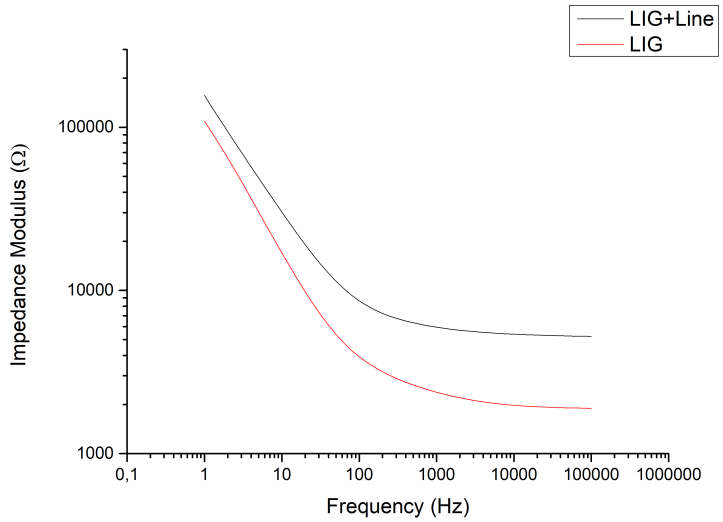

FIGURE 4.15: Vertical shift of the modulus of the EIS due to the increased resistivity given by the LIG tracks.

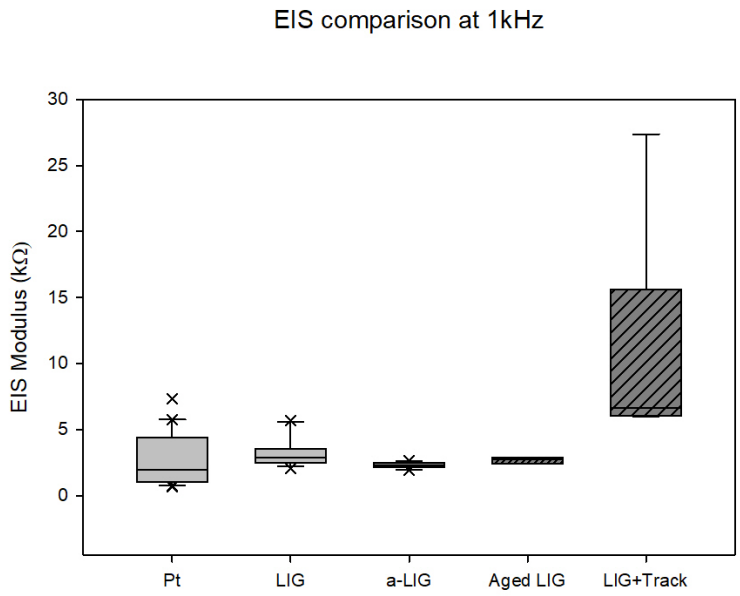

FIGURE 4.16: Comparison of EIS values for samples

As it can be seen, the conductivity of platinum is sensibly lower than copper, which is a much better conductor; however for biological applications copper cannot be used for toxicity reasons, therefore the larger resistivity of platinum is necessary to have a biologically safe implantable device.
The resistivity for LIG has been calculated by evaluating the median of all measured samples and it is several orders of magnitude higher than that of a metal. The great advantage of having an all-LIG device therefore could be impaired by the excess of resistivity of the lines connecting the stimulation electrodes to the external circuitry, causing an excessive dissipation of power and an unsustainable voltage drop on the tracks. This higher resistivity however is partially compensated by the improved mechanical properties of laser induced graphene on polyimide, such as flexibility, or even stretchability and elasticity in the case of transferring the LIG network to a PDMS substrate.

As a consequence, the contribution of LIG tracks on the electrochemical properties of such electrodes is highly detrimental, strongly increasing the electrochemical impedance modulus value due to the resistivity of the tracks contacting the electrodes. Unfortunately the negative effects of the tracks is not limited only to the impedance, but it has an impact also on the charge storage capacity of LIG electrodes at the interface with PBS.
Figures 4.16 and 4.17 show the comparison of LIG electrodes in all tested conditions with standard platinum: as already mentioned the results for EIS are roughly five times bigger than electrodes only, while the results of the cyclic voltammetries performed including the tracks in the conductive path show a significant decrease in charge storage capacity. The effects of resistivity brought the CSC to the values of LIG prior to activation, which are almost equivalent to those of platinum.

If one considers that the LIG is an all-carbon material with great mechanical properties in terms of flexibility, which would highly reduce the mechanical mismatch between

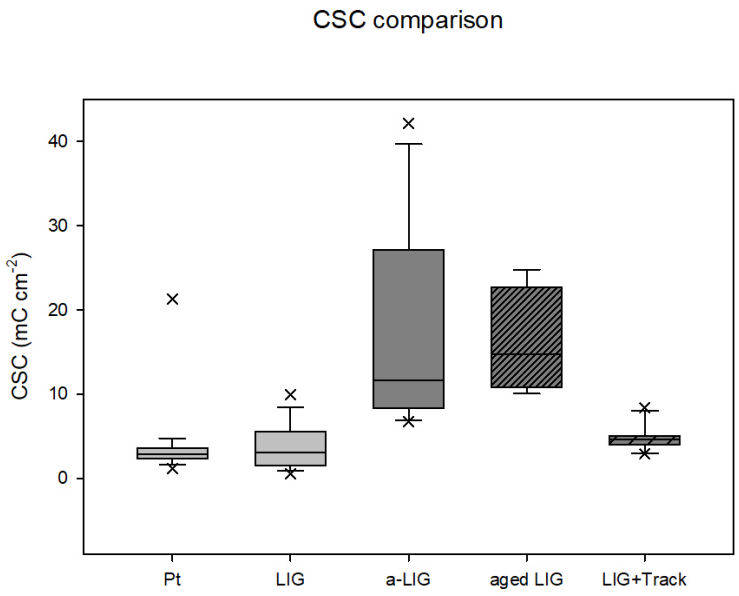

FIGURE 4.17: Comparison of CSC values.

the stimulating electrode and the neural tissue, and good biocompatibility, a charge storage capacity comparable with platinum could already guarantee a good enough performance to try to pursue the use of LIG electrodes in implantable devices.

4.1.3 Stimulation pulsing

Considering the results of cyclic voltammetry and electrochemical impedance spectroscopy performed on all three kinds of graphene-based electrode, it can be clearly seen that the few layer graphene samples, although quite promising from the graphene fabrication point of view, did not quite achieve the desired properties, with extremely high impedance if compared to other tested samples 4.11 and very low charge storage capacity.

Single layer graphene showed better performances with respect to the few layered structures, but according to the Raman spectra of SLG transferred to platinum substrates the coating of the metallic surface has not been successful, leaving many regions of the substrate exposed to the electrolyte. Since no measurements of a uniform and continuous coating of SLG on platinum has been made in this study, it is not possible to deduce the effects of such a structure when it interacts with platinum and with a neural tissue or an electrolyte for preliminary in-vitro tests. It would definitely increase the biocompatibility of the implanted electrode and could allow for integration of different features due to its many different properties, such as optical or thermal. However, limited to this study, considering also the difficulty of fabrication and of the transfer process to the native copper substrate to the platinum surface, the problems of creating a stable electrical contact with a metallic wire through welding, both the SLG and the FLG have not been studied

for what concerns the preliminary measurements performed to evaluate the charge injection capacity.

The stimulation pulses are delivered through a custom made device which can deliver current pulses of given peak current and pulse width. The shape of the pulse width is a squared wave with cathodic first phase and a short interphase period of constant value. As for previous measurements also platinum electrodes have been tested, besides the LIG ones, in order to obtain a consistent set of measurements for comparison. The voltage response is measured with a digital oscilloscope averaging between four periods to reduce the noise.
First, the charge injection capacity has been calculated by setting the pulse width to 100 µs and increasing the current until the value of E_{mc} reached -0.6 V, which is the most negative potential allowed in a platinum electrode before causing water hydrolysis.The charge injection capacity is then calculated as the current flowing through the electrode times the pulse width divided by the exposed area of the electrode.
The same procedure has been done for platinum and activated LIG electrodes, varying the current from 100 µA to the values that caused a maximum negative residual polarization of -0.6V. For what concerns LIG electrodes the current has been increased further since the activation protocol performed before the cyclic voltammetry measurements showed that water hydrolysis at the electrode-electrolyte interface in the case of LIG electrodes did not occur at voltages of -1.4 V. Therefore the current has been increased until the value of E_{mc} did not reach -1.2 V, which ensures a safe margin from the dissolution of water and creation of reactive species, gas bubbles that could impair the measurements and damage the biological environment. This is a major advantage of laser induced graphene electrodes over other types of samples: the presence of only graphene flakes onto a polymeric substrate, completely avoiding the presence of a platinum electrode, allows to safely polarize the sample to higher values of voltage. Even though, in hypothesis, the SLG or FLG could allow for a wider potential window before water hydrolysis, the presence of the platinum substrate would suggest to limit the applied potential to the standard platinum water window (-0.6, 0.8) V, since a minor discontinuity or defect in the graphene layer would expose the platinum, which if polarized outside its water window could produce dangerous species and ultimately damage or destroy the graphene coating. As instead LIG electrodes do not contain any platinum, which allows for a safe polarization of the electrode to its full potential, without the risk of unwanted reactions.

Figure 4.18 shows the voltage pulses used to calculate the CIC for the two different potential limits E_{mc}.

By changing the pulse width of the current pulses and evaluating the charge injection capacity, it is possible to find the relation between the duration of the pulse and the CIC. As stated by Cogan, the charge injection capacity is found to be increasing with longer pulses[12], both for platinum and LIG electrodes. As it can be seen in figure 4.19, the logarithm of the CIC is increasing with the pulse width, roughly doubling its value when

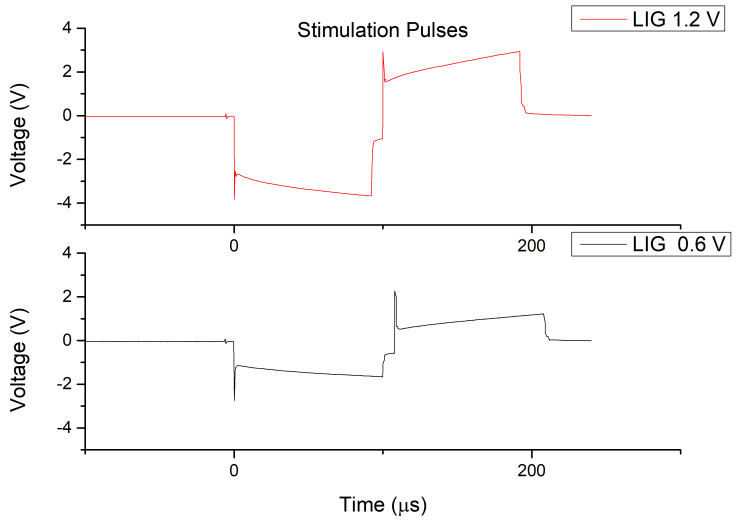

FIGURE 4.18: LIG response to stimulation pulse with E_{mc} equal to -1.2V and 0.6 V.

changing the pulse from 50 µs to 500 µs. The increase is more noticeable with the LIG samples, especially with the wider potential window, due also to the porous structure of the LIG. When the frequency of the pulsing is decreased, the ionic charges have a better chance to penetrate into the pores and to flow through the channels and exchange charge, therefore the relative increase in the LIG is much more evident than the platinum electrodes.

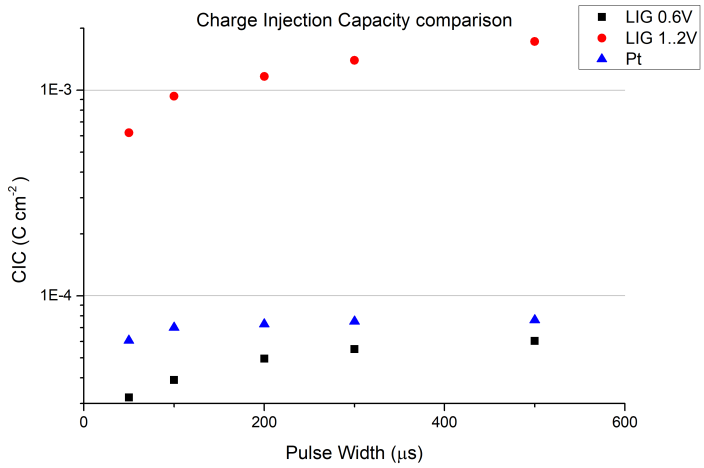
Charge Injection Capacity comparison
LIG 0.6V
LIG 1..2V
Pt
1E-3
1E-4
CIC (C cm-2)
0
200
400
600
Pulse Width (µs)

FIGURE 4.19

Chapter 5

Conclusions

The work presented here describes the study of graphene-based electrodes for neural applications, concerning the fabrication, the characterization of the obtained materials and the measurement of electrochemical properties related to neural stimulation and signal recording.

The study had two major areas of interest: the first was performed at Politecnico di Torino and focused on the fabrication of single layer graphene and few layers graphene with thin film technology and the direct writing of laser induced graphene on polymeric substrates, followed by the physical and chemical characterization of the structures. The samples were then brought to the Bionics Institute of Melbourne to evaluate the electrochemical properties of the graphene-based samples.

This work will allow a better understanding of the possibilities of employing graphene and related materials in stimulation and recording applications, understanding the strengths and weaknesses of these materials: although many steps required to create a fully implantable device are still to be made, this study shows the potentiality of graphene-based electrodes in realizing an implant with greater biocompatibility, mechanical and electrical properties.

5.1 Achievements

The work developed during this project gave many interesting results.

For what concerns the fabrication, the process of growing graphene directly on platinum was successfully developed and the studies were made on the transfer of graphene, from the growing copper substrate to the platinum electrodes. These studies led to the understanding of the problems and limitations of graphene layers on metallic substrates, which consist in the damaging of graphene during the transfer process and the difficulties in connecting such electrodes to metallic wires.

The electrochemical properties have been thoroughly evaluated, determining the differences between the three types of graphene and comparing them to an internal control,

represented by the standard material for neural devices which is platinum. The problems encountered with the fabrication of SLG and FLG were reflected onto the electrochemical properties, providing results of CSC and electrochemical impedance that did not improve with respect to platinum.

Considering LIG electrodes the measurements of properties and performances showed great results: the tested samples had large charge storage capacity and lower impedance than platinum, confirmed by the long term stability measurements of the accelerated aging protocol. A final test of stimulation pulses was performed in order to determine the charge injection capacity of the material, yielding great results also due to the absence of any metallic component exposed to the electrolyte, allowing for a greater potential window.

Although many problems have to be solved, such as the high resistivity of LIG tracks, and many questions have to be answered, laser induced graphene seems a great potential candidate for implantable devices: it can be directly written on a biocompatible polymeric substrate, allowing for great versatility and flexibility in the design of the array and in the prototyping of the system, with no need for manual craftsmanship to assemble platinum arrays.

5.2 Future outlook

This work left many unanswered questions that will be further studied.

First of all the accelerated aging protocol is currently in progress, in order to evaluate the possibility of chronic implantation.

The next measurements to be performed are chronic pulsed stimulation in vitro with the goal of defining the stability of the material when subjected to long term electrochemical stress.

From the device perspective, the main target will be to reduce the resistivity of the LIG tracks that could impair the efficacy of the implant; integration of metallic lines connecting the LIG electrodes to the external circuitry directly deposited on the polymeric substrate could be a viable solution if the mechanical properties of flexibility will be ensured. Alternatively the conductivity of LIG tracks could be increased by conductive polymer intercalation, such as PEDOT:PSS, platinum sputtering or electrodeposition.

Different types of laser induced graphene, shown in section 3.1.3, could be tested, in order to verify if the chosen morphology provides indeed the best electrochemical performances.

The ultimate goal, once the engineering of the implant will be completed, allowing for a stable and reliable connection of the LIG electrodes to the external electronics and the encapsulation of the lines exposing the electrodes only, is to perform pre-clinical in-vivo experiments, in order to evaluate the response of the system to a real biological environment.

Bibliography

[1] In:

[2] Ulises A Aregueta-Robles et al. “Organic electrode coatings for next-generation neural interfaces”. In: *Frontiers in neuroengineering* 7 (2014), p. 15.

[3] Danny Banks. “Neurotechnology”. In: *Engineering Science and Education Journal* 7.3 (1998), pp. 135–144.

[4] Allen J Bard et al. *Electrochemical methods: fundamentals and applications*. Vol. 2. wiley New York, 1980.

[5] B. Bonaz et al. “Chronic vagus nerve stimulation in Crohn’s disease: a 6-month follow-up pilot study”. In: *Neurogastroenterology & Motility* 28.6 (2016), pp. 948–953. DOI: 10.1111/nmo.12792.

[6] J. H. Brannon et al. “Excimer laser etching of polyimide”. In: *Journal of Applied Physics* 58.5 (1985), pp. 2036–2043. DOI: 10.1063/1.336012.

[7] James Cavuoto. “Commercial opportunities for neural engineers”. In: *Journal of Neural Engineering* 5.1 (2008).

[8] CH Chen et al. “A graphene-based microelectrode for recording neural signals”. In: *Solid-State Sensors, Actuators and Microsystems Conference (TRANSDUCERS), 2011 16th International*. IEEE. 2011, pp. 1883–1886.

[9] Nuan Chen et al. “Neural interfaces engineered via micro-and nanostructured coatings”. In: *Nano Today* 14 (2017), pp. 59–83.

[10] Hyun-Jung Choi et al. “Graphene for energy conversion and storage in fuel cells and supercapacitors”. In: *Nano Energy* 1.4 (2012), pp. 534–551.

[11] Stuart F Cogan. “Microelectrode coatings for neural stimulation and recording”. In: *Engineering in Medicine and Biology Society, 2003. Proceedings of the 25th Annual International Conference of the IEEE*. Vol. 4. IEEE. 2003, pp. 3798–3801.

[12] Stuart F Cogan. “Neural stimulation and recording electrodes”. In: *Annu. Rev. Biomed. Eng.* 10 (2008), pp. 275–309.

[13] David Cohen-Tanugi and Jeffrey C Grossman. “Water desalination across nanoporous graphene”. In: *Nano letters* 12.7 (2012), pp. 3602–3608.

[14] Zengxin Dai et al. “Cell voltage versus electrode potential range in aqueous supercapacitors”. In: *Scientific reports* 5 (2015), p. 9854.

[15] J. Davenas. "Laser and ion beam processing of conductive polyimide". In: *Applied Surface Science* 36.1 (1989), pp. 539 –544. DOI: https://doi.org/10.1016/0169-4332(89)90948-3.

[16] Xiaowei Du et al. "Graphene microelectrode arrays for neural activity detection". In: *Journal of biological physics* 41.4 (2015), pp. 339–347.

[17] *Electrochemical Single-core Microelectrodes*. URL: http://www.thomasrecording.com/products/electrochemical-products/electrochemical-microelectrodes/electrochemical-single-core-microelectrodes.html.

[18] Christoph Fenzl et al. "Laser-Scribed Graphene Electrodes for Aptamer-Based Biosensing". In: *ACS Sensors* 2.5 (2017), pp. 616–620. DOI: 10.1021/acssensors.7b00066.

[19] A. C. Ferrari et al. "Raman Spectrum of Graphene and Graphene Layers". In: *Phys. Rev. Lett.* 97 (18 2006), p. 187401. DOI: 10.1103/PhysRevLett.97.187401.

[20] Andrea C Ferrari et al. "Science and technology roadmap for graphene, related two-dimensional crystals, and hybrid systems". In: *Nanoscale* 7.11 (2015), pp. 4598–4810.

[21] David J Garrett et al. "Ultra-nanocrystalline diamond electrodes: optimization towards neural stimulation applications". In: *Journal of neural engineering* 9.1 (2011), p. 016002.

[22] RA Green et al. "Performance of conducting polymer electrodes for stimulating neuroprosthetics". In: *Journal of neural engineering* 10.1 (2013), p. 016009.

[23] Rylie A Green et al. "Conducting polymer-hydrogels for medical electrode applications". In: *Science and Technology of Advanced Materials* 11.1 (2010), p. 014107.

[24] Rylie A Green et al. "Conducting polymers for neural interfaces: challenges in developing an effective long-term implant". In: *Biomaterials* 29.24-25 (2008), pp. 3393–3399.

[25] Rylie A Green et al. "Substrate dependent stability of conducting polymer coatings on medical electrodes". In: *Biomaterials* 33.25 (2012), pp. 5875–5886.

[26] Gita Handa. "Neural prosthesis–past, present and future". In: *Indian Journal of Physical Medicine & Rehabilitation* 17.1 (2006), p. 460.

[27] Rachelle T Hassarati et al. "Improving cochlear implant properties through conductive hydrogel coatings". In: *IEEE Transactions on Neural Systems and Rehabilitation Engineering* 22.2 (2014), pp. 411–418.

[28] National Institutes of Health. *Cochlear Implants*. Online; accessed 26 January 2018. 2017. URL: https://www.nidcd.nih.gov/health/cochlear-implants.

[29] Chaejeong Heo et al. "The control of neural cell-to-cell interactions through non-contact electrical field stimulation using graphene electrodes". In: *Biomaterials* 32.1 (2011), pp. 19–27.

[30] Christie Q Huang, Paul M Carter, and Robert K Shepherd. "Stimulus induced pH changes in cochlear implants: an in vitro and in vivo study". In: *Annals of biomedical engineering* 29.9 (2001), pp. 791–802.

[31] A K. N. Geim and K. S. Novoselov. "The Rise of Graphene". In: 6 (Apr. 2007), pp. 183–91. DOI: 10.1038/nmat1849.

[32] Berit Koerbitzer et al. "Graphene electrodes for stimulation of neuronal cells". In: *2D Materials* 3.2 (2016), p. 024004.

[33] Andrea Lamberti et al. "A Highly Stretchable Supercapacitor Using Laser-Induced Graphene Electrodes onto Elastomeric Substrate". In: *Advanced Energy Materials* 6.10 (2016), 1600050–n/a. DOI: 10.1002/aenm.201600050.

[34] Andrea Lamberti et al. "New insights on laser-induced graphene electrodes for flexible supercapacitors: tunable morphology and physical properties". In: *Nanotechnology* 28.17 (2017), p. 174002.

[35] Brian Lee, Charles Y. Liu, and Michael L.J. Apuzzo. "A Primer on Brain–Machine Interfaces, Concepts, and Technology: A Key Element in the Future of Functional Neurorestoration". In: *World Neurosurgery* 79.3 (2013), pp. 457 –471. DOI: https://doi.org/10.1016/j.wneu.2013.01.078.

[36] Jian Lin et al. "Laser-induced porous graphene films from commercial polymers". In: *Nature Communications* 5 (2015). DOI: 10.1038/ncomms6714.

[37] Yichen Lu et al. "Flexible neural electrode array based-on porous graphene for cortical microstimulation and sensing". In: *Scientific reports* 6 (2016), p. 33526.

[38] Sida Luo, Phong Tran Hoang, and Tao Liu. "Direct laser writing for creating porous graphitic structures and their use for flexible and highly sensitive sensor and sensor arrays". In: *Carbon* 96 (2016), pp. 522 –531. DOI: https://doi.org/10.1016/j.carbon.2015.09.076.

[39] Yvonne H.-L. Luo and Lyndon da Cruz. "A review and update on the current status of retinal prostheses (bionic eye)". In: *British Medical Bulletin* 109.1 (2014), pp. 31–44.

[40] LM Malard et al. "Raman spectroscopy in graphene". In: *Physics Reports* 473.5-6 (2009), pp. 51–87.

[41] *Modeling Electroanalysis: Cyclic Voltammetry*. URL: https://www.comsol.com/blogs/modeling-electroanalysis-cyclic-voltammetry/.

[42] Jungtae Nam et al. "Chemical vapor deposition of graphene on platinum: Growth and substrate interaction". In: *Carbon* 111 (2017), pp. 733 –740. DOI: https://doi.org/10.1016/j.carbon.2016.10.048.

[43] Sandeep Negi, Rajmohan Bhandari, and Florian Solzbacher. "A novel technique for increasing charge injection capacity of neural electrodes for efficacious and safe neural stimulation". In: *Engineering in Medicine and Biology Society (EMBC), 2012 Annual International Conference of the IEEE*. IEEE. 2012, pp. 5142–5145.

[44] Sandeep Negi et al. "Neural electrode degradation from continuous electrical stimulation: Comparison of sputtered and activated iridium oxide". In: *Journal of Neuroscience Methods* 186.1 (2010), pp. 8 –17. DOI: https://doi.org/10.1016/j.jneumeth.2009.10.016.

[45] K. S. Novoselov et al. "Electric Field Effect in Atomically Thin Carbon Films". In: *Science* 306.5696 (2004), pp. 666–669. DOI: 10.1126/science.1102896.

[46] Bart Partoens and FM Peeters. "From graphene to graphite: Electronic structure around the K point". In: *Physical Review B* 74.7 (2006), p. 075404.

[47] *Resistivity and Temperature Coefficient at 20 C*. URL: http://hyperphysics.phy-astr.gsu.edu/hbase/Tables/rstiv.html.

[48] Mingyu Ryu et al. "Enhancement of interface characteristics of neural probe based on graphene, ZnO nanowires, and conducting polymer PEDOT". In: *ACS Applied Materials & Interfaces* 9.12 (2017), pp. 10577–10586.

[49] Weixing Song et al. "Flexible, Stretchable, and Transparent Planar Microsupercapacitors Based on 3D Porous Laser-Induced Graphene". In: *Small* 14.1 (2018). DOI: 10.1002/smll.201702249.

[50] R. Srinivasan, B. Braren, and R. W. Dreyfus. "Ultraviolet laser ablation of polyimide films". In: *Journal of Applied Physics* 61.1 (1987), pp. 372–376. DOI: 10.1063/1.338834.

[51] R. Srinivasan et al. "Formation of a Porous, Patternable, Electrically Conducting Carbon Network by the Ultraviolet Laser Irradiation of the Polyimide PMDA-ODA (Kapton)". In: *Chemistry of Materials* 6.7 (1994), pp. 888–889. DOI: 10.1021/cm00043a005.

[52] Veronica Strong et al. "Patterning and Electronic Tuning of Laser Scribed Graphene for Flexible All-Carbon Devices". In: *ACS Nano* 6.2 (2012), pp. 1395–1403. DOI: 10.1021/nn204200w.

[53] Peter Sutter, Jerzy T. Sadowski, and Eli Sutter. "Graphene on Pt(111): Growth and substrate interaction". In: *Phys. Rev. B* 80 (24 2009), p. 245411. DOI: 10.1103/PhysRevB.80.245411.

[54] Mingliang Tang et al. "Enhancement of electrical signaling in neural networks on graphene films". In: *Biomaterials* 34.27 (2013), pp. 6402–6411.

[55] Thomas Wells. *Determining the voltage range of a carbon-based supercapacitor*. 2014.

[56] Joost Wintterlin and M-L Bocquet. "Graphene on metal surfaces". In: *Surface Science* 603.10 (2009), pp. 1841–1852.

[57] A to Z research. *Cardiac Pacemaker Market by Product (Implantable Cardiac Pacemaker and External Cardiac Pacemaker) Analysis and Forecast by 2021*.

[58] Jibo Zhang et al. "Efficient Water-Splitting Electrodes Based on Laser-Induced Graphene". In: *ACS Applied Materials & Interfaces* 9.32 (2017), pp. 26840–26847. DOI: 10.1021/acsami.7b06727.